Corrosion Behavior of the Cladding Tube (AISI Type-316SS) for FBR in High Temperature Sodium

(1) Experimental Studies on Effects of Oxygen Concentration in Sodium on Corrosion

July 1976

POWER REACTOR AND NUCLEAR FUEL DEVELOPMENT CORPORATION

PNC TN951 76-07
July, 1976

Corrosion Behavior of the Cladding Tube (AISI Type-316SS) for FBR in High Temperature Sodium

(1) Experimental Studies on Effects of Oxygen Concentration in Sodium on Corrosion

Shun-ichi Yuhara*,
Shigeki Kanoh*,
Tetsuro Owada*, and
Hideo Atsumo*

Abstract

Some experimental studies were carried out to study the effects of oxygen concentration in sodium on corrosion for the domestic cladding tube (nominal dimension of 6.3 mm outside diameter at 0.35 mm wall thickness) of Type-316 stainless steel. The daughter loops, M-2 and M-11, were used for mass-transfer test of the tube specimen, in which the test condition was individually selected on the oxygen concentration; the cold trap temperatures were controlled at 200 °C in M-2 and 150 °C in M-11. Mass-transfer test was done for about 2,000 hours in flowing sodium and the maximum temperature of test sections was held at 650 °C. After exposure in sodium, the following analyses were made on the specimens: weighing, surface roughness, SEM, X-ray diffraction, X-ray microprobe, mechanical properties and others.

The results are summarized as follow:

---

* Sodium Technology Section, Sodium Engineering Division, O-arai Engineering Center.

(1) General corrosion rate of the cladding tube specimen is remarkably dependent on the oxygen concentration. It shows distinguished increase as the cold-trap temperature increases.

(2) The iron rich layer was observed, where nickel and chromium were depleted. Elemental leaching and depletion in the surface layer were mainly observed inwards along the grain boundary in the neighbour of the surface exposed in sodium. Thickness of the leaching layer was about 30 μm.

(3) At the surface layer of the specimens exposed in sodium, the presence of ferrite was confirmed by X-ray diffraction, and the surface roughness of the specimens after exposure in the higher oxygen concentration increased to about 1.8 times as large as those before exposure.

CONTENTS

List of Figures

List of Tables

List of Photos

1. Introduction

The decrease in the thickness and property change of surface layer of the cladding tube for FBR due to corrosion in high-temperature flowing sodium are dependent on various parameters of the corrosive environment, such as the purity of sodium. Experimental evaluation of them is considered to be important, in view of the effect of corrosion on the material strength of thin-wall and small-diameter tubes of a fuel assembly. For this reason it is required to evaluate experimentally sodium corrosion behavior of domestically produced cladding tubes.

In order to investigate the effect of the oxygen concentration in sodium on the corrosion of the cladding tube, two different loops (M-2 daughter loop in the low-purity material test loop and M-11 daughter loop in the medium-purity material test loop) were used, where the test condition can be individually selected on the oxygen concentration in sodium. The sodium exposure test on the JOYO fuel cladding tubes will carried out at the maximum sodium temperature of 650 °C and two different oxygen concentrations in sodium (cold trap temperatures 200 °C and 150 °C) up to 2062 hours.[Note 1)] The amount of decrease in thickness of the cladding tube was obtained and a study of the effect of the decrease in thickness on material strength was made. Furthermore, some experiments were carried out on the 650 °C exposed specimens (cladding tube) to reveal the corrosion behavior, such as forms of the corroded surface layer, the leaching and depletion of alloying elements in the grain boundary, and the changes in mechanical properties after exposure in sodium.

Note 1): Afterward, some of the specimens were exposed to sodium up to 3063 hours.

The data relating to the rate of decrease in thickness of the cladding tube due to exposure in sodium and the depth of depletion layer will be valuable in making strict evaluation of the decrease in creep strength and so on in future.

2. Cladding Tube Specimens, Test Apparatus and Procedures

2.1 Cladding tube, and shape of the specimens

The cladding tubes tested in sodium were made of Type AISI-316 austenitic stainless steel (the amounts of B, N and Co were specified). The chemical composition, grain size number and cold working rate are shown in Table 1. The cladding tube specimens were manufactured and heat-treated as below.

Steelmaking → ingot making → billeting → extrusion → rolling → drawing → heat treatment (bright annealing at 1,000 °C ~ 1,100 °C) → final cold drawing → rolling → straightening → tube

Table-1 Material properties of Type-316 stainless steel cladding tube

Chemistry / Analysis	C	Si	Mn	P	S	Cu	Ni	Cr	Mo	Co	B	N
Ladle analysis	0.06	0.58	1.52	0.003	0.017	0.23	13.14	16.60	2.52	0.02	0.0005	0.042
Check analysis	0.06	0.56	1.52	0.003	0.013	0.22	13.14	17.05	2.40	0.02	0.0002	0.0262
〃	0.06	0.56	1.53	0.003	0.013	0.22	13.15	17.00	2.41	0.02	0.0002	0.0260

Grain size number ASTM No. 7.1 7.0, Cold working rate 10 12 %
Cladding tube form 6.3φ (O.D.) x 5.6φ (I.D.)

Two types of specimens used for mass transfer test are shown in Fig. 1. Specimen A has welded plugs at both ends for making investigations on the corrosion of the welding zone. Specimen B is for making investigations on the corrosion behavior, mainly the changes in the wall thickness (mass transfer) of the fuel cladding tube. When inserted into the loop, the specimen is fixed by means of the filler piece. A pair of specimens A and B is inserted in each of the test sections (T - 1 T - 5 in Fig. 5)

2.2 Test apparatus (soium loop)

The test apparatus used in this experiment comprises the daughter loops M-2 and M-11 branched from two mother loops respectively (low-purity material test loop and medium-purity material test loop). The flow sheets of the loops M-2 and M-11 are shown in Fig. 2. Each mother loop is composed of a purifying line with a cold trap, a plugging indicator line, an oxygen meter line, mass transfer test sections, creep test sections and so on.
As shown in Fig. 2, the daughter loop for mass transfer test is composed of an AC Faraday type electromagnetic pump, an electromagnetic flow meter, an immersion heater, a fan cooler and five freeze-seal type test sections. These are the monometallic type loops entirely made of SUS-316, equivalent to AISI-316 (the mother loop is entirely made of SUS-304, equivalent to AISI-304).
Photo-1 shows part of the mass transfer test loop (M-11).

2.3 Test conditions of sodium exposure

The sodium exposure test was carried out while constantly supplying the daughter loops with refined sodium from the mother loops. The sodium exposure test conditions used in our experiments are listed in Table 2.

As shown in this table, two conditions were selected for the oxygen concentration in sodium (cold trap temperature: 200 °C and 150 °C). The test section T-1 of the M-11 loops has the maximum temperature 650 °C and the maximum sodium velocity 6.0 m/sec.[Note 2)]

Note 2): The sodium velocity in M-2 was originally set at 6 m/sec but we used a velocity of 2.6 m/sec due to the restrictions imposed by the capacity of the electromagnetic pump. In view of the results, two units of pumps approximately equal to the one used for M-2 were installed in M-11 in order to obtain a larger capacity.

among all the test sections. The specimens which were exposed in sodium at the cold trap temperature of 200 °C (oxygen concentration: 5 ppm) will be referred to as the high-oxygen exposure specimen and the low-oxygen exposure specimen respectively.

Table-2 Test conditions in flowing sodium

Test condition / Mother loop	Daughter loop	Max. sodium temperature	Sodium velocity	Cold trap temperature	O_2 concentration (wppm)	Exposed time
Low Purity Material Test Loop	M − 2	650 ℃ (T − 1)	2.6m/sec (T − 1)	200 ℃	12 (Chemical analysis value)	953 [hr]
Medium Purity Material Test Loop	M −11	650 ℃ (T − 1)	6.0m/sec (T − 1)	150 ℃	5 (Chemical analysis value)	904 2069 hr

2.4 Testing procedures after sodium exposure

After exposure in sodium with two different oxygen concentrations, some tests were conducted on the specimens to investigate surface corrosions (i, ii, iii, iv and v), the internal corrosion (vi, vii), and the effect of corrosion on the mechanical properties of the cladding tube (viii) as described below.

(i) Weighing of specimens after sodium exposure

After exposed to sodium, the specimens were ultrasonically cleaned in ethyl alcohol and dried by hot air before weighing. An H-20 direct-indication balance (made by Mettler Co.) was used for weighing the specimens. This balance is capable of weighing up to 160 g and the minimum reading is 1/100 mg.

(ii) Scanning electron microscopy

The scanning electron microscopic observations were made

using an HSM-2 scanning electron microscope with a resolving power of 200 Å of all the specimens as received or after exposure in sodium without any surface treatment such as metal evaporation coating. Scanning electron micrographs were taken under the conditions as an accelerating voltage of 25 kV, an inclination angle of 45 ° - 30 °, an exposure time of 100 seconds and a magnification of 400 X - 20,000 X. The ruptured surfaces after the ring tensile test were also observed by the same procedures under the same conditions.

(iii) Surface roughness test

The surface roughness test was carried out to determine the surface roughness before and after sodium exposure, using the needle-touch type super roughness tester AB-2 (made by Mitsutoyo Seisakusho). This is a type of surface roughness tester by which the vertical displacements of the tip of the needle are detected by a strain gauge. The needle tip is made of diamond with a diameter of 5 μm and an angle of 70 °. It, therefore, shows a value slightly smaller than the actual depth of depressions less than 5 μm. The test was made by tracing the surface of the cladding tube specimen with the needle along the longitudinal direction.

(iv) X.M.A. (X-ray microanalysis test of sodium exposed surfaces

In order to investigate the forms of the corroded surfaces and the changes in the concentrations of alloying elements in the surface layer, X-ray microanalysis (XMA) was made to obtain the characteristic X-ray images and line using profiles of the surface of the cladding tube specimens, XMA-5 microanalyzer (made by Hitachi, Ltd.), which has three detectors so that three elements may be linearly analyzed simultaneously. The X-ray microanalysis was

carried out for such combinations of elements as Ni, Cr and C, for example. Analyses were made on such elements as Fe, Ni, Cr, Mo, Na, C, O and N. The method of the line scanning used in the XMA line analysis is illustrated in Fig. 5. To examine the changes in the concentrations of elements in the surface layer and in the interior, the line analysis was made on the surface exposed in sodium and the region in which the surface was ground to a depth of approx. 50 μm to 100 μm. The XMA test conditions are presented in Table 3.

Table-3 Conditions of characteristic X-ray analysis

Element	Characteristic Xray	Cryostat	Accelerating Voltage	Specimen Absorbtion Current	Ramarks
Fe	K_α	Li-F	20kV	0.05 μA	
Ni	K_α	Li-F	〃	〃	
Cr	K_α	Li-F	〃	〃	
Mo	K_α	※1 ADP	〃	〃	※1 $NH_4H_2PO_4$
C	K_α	※2 STE	〃	〃	※2 $Pb(C_{17}H_{35}COO)_2$
Na	K_α	※3 KAP	〃	〃	※3 $C_6H_4\begin{pmatrix}COOH\\COOK\end{pmatrix}$
O	K_α	STE	〃	〃	
N	K_α	〃	〃	〃	

(v) X-ray diffraction of the surface exposed to sodium

X-ray diffraction test was carried out to investigate the changes in the crystal structure of the corroded surface of the cladding tube specimen. The apparatus is a self-recording X-ray diffractometer (made by Rigaku Denki) composed of an X-ray generator 4053A3, a diffraction goniometer SG-8, a counting and recording device 5055A, and an NaI scintillator. The cladding tube specimen for diffraction test was sliced to a

length of 20 mm, compressed flat by use of the Instron tensile tester and fixed to an aluminum plate. Cu($K\alpha$) rays were used in the diffraction test and the diffraction patterns from the various diffraction planes as (110) plane were recorded. The test conditions were as follows.

Target X-ray	Cu$K\alpha$
Applied voltage	30kV
Coarse Gain	2
Scanning speed	1 °/min. ~ 4 °/min.
Chart speed	10mm/min. ~ 20 mm/min.
Full scale	2×10^3 c/sec.
Time constant	1 sec. ~ 0.5 sec.

(vi) X-ray microanalysis of the longitudinal sections of cladding tube specimens

In order to investigate the corrosion behavior (leaching and depletion) at the sections of cladding tube specimens, the distribution of alloying elements was measured using an X-ray microanalyzer. The analyses were made by use of the same method and apparatus as in the case of the sodium exposed surfaces. The beam scanning for the X-ray analysis was carried out in the longitudinal direction of the specimen. The sandwitch method illustrated in Fig. 6 was adopted to minimize the "slacking" of the specimen end. Embedded in resin and buffed to 0.05 μm, the specimen was removed from the resin bed and then the X-ray scanning was carried out parallel to the sodium exposed surface at a specified depth. By repeating this procedure in the direction of depth, the distributions of alloying element concentrations were measured from the surface to the inner section

of the specimen.

(vii) Metallographic test of the sections of specimens

To make observations of the micro-structure, the specimen was sandwitched and embedded in resin as in the case of (vi). After polished with emery paper and buffed, the specimen was etched with aqua regina. For the metallographic test after tensile rupture, the specimen was first plated with nickel to prevent the "slacking" of the specimen end in polishing, embedded in resin and thereafter the same method as described above was used for observation.

(viii) Ring tensile test

An Instron tensile tester (TT-CM-1) was used to carry out the ring tensile test with a tensile velocity of 0.5 mm/min. (cross-head speed) at room temperature in the air. The specimen for this test was prepared as described below. The specimen was first sliced about 1.4 mm wide, using a presion cutter (with a thin cutting edge of 0.5 mm) and the test piece was ground to the accuracy of 1.000 ±0.005 mm by the use of wet emery paper.

3. Results

3.1 Weight loss of the metal dissolution in 650 °C sodium

Fig. 7 shows the relation between the decrease of weight due to the metal loss of the FBR fuel cladding tube specimen in flowing sodium with low oxygen concentration (cold trap temperature: 150 °C, oxygen concentration: 5 ppm) at 650 °C and the duration of exposure of the specimen in sodium. Under these conditions, the initial corrosion within about 1,000 hours did not seem to be so remarkable. The relation between the cold trap temperature (corresponding to the oxygen concentration in sodium) and the rate of metal loss, i.e., the rate of thickness decrease is shown in Fig. 8. It is evident from this figure that the metal loss increases as the cold trap temperature increases, i.e., the oxygen concentration increases. This tendency agrees with the tendencies obtained by other investigators.[3][4][5] The scattering of data relating to the type of specimen exposed to the low oxygen sodium in Fig. 7 seems presumably to be within the experimental results. One of the causes of the difference between the data of the specimens exposed to the high oxygen sodium is presumably that in the case of B type specimens the influence of sodium penetration between the filler piece and the inside of the cladding tube was greater on the specimen exposed to the high oxygen sodium than on the specimen exposed to the low oxygen sodium, and consequently noticeable difference was brought in weight changes. Investigations are being made on the cause of this phenomenon and a study is also being made on improving the form of the specimens to minimize the scattering of the corrosion rate data.

3.2 Scanning electron microscopy of surface corrosion

Photo 2 shows the scanning electron micrographs of the surface of cladding tube specimen before exposure to sodium. As seen from Photo 2(a), the surface of the cladding tube shows only the minute abrasions presumably made during its final machining and the surface condition is good. Photos 2(b) and (c) show further magnified views of the surface. The maximum height of the surface roughness (JIS) was 0.9 μm. Photo 3 shows the surface corrosion after sodium exposure. Photos 2(A), 2(D) and 2(E) show the surface corrosion after sodium exposure. Photos 3(A), 3(D) and 3(E) show the surface of the tube, while Photos 3(B) and 3(C) show the heat-affected zone of the welded end plug. Photos 3(C) and 3(E) are the micrographs of higher magnifications of the same places with (B) and (D). The surface corrosion showed the general characteristics as follows: (i) The grain boundary appears distinctly and is slightly depressed compared with the matrix. Noticeable intergranular corrosion is not observed and the main corrosion morphology is considered to be the general corrosion. (ii) Corrosion products of about 0.2 μm to 1 μm in size are observed on the surface of the matrix. (iii) The degree of corrosion varies slightly along the direction of the individual crystal grains in the surface, which may be related to the wavelike surface roughness. (iv) Both welded and heat-affected zones have no noticeable difference as compared with the tube surface except the welded part (refer to Photos 3(A), 3(B) and 3(C). (v) On the oxygen concentration dependence of corrosion, the corroded surface is more crystalline.

3.3 Surface roughness change due to sodium exposure

The surface roughness data before and after sodium exposure are shown in Fig. 9. The specimen exposed to the high oxygen concentration sodium (1,000 hrs.) had a greater surface roughness change than it in the low oxygen concent ration sodium (2,000 hrs), with an increase to 1.6 μm (the mean value of roughness according to the maximum height indication) from the roughness of 0.9 μm before sodium exposure. In the case of the specimen exposed to the low xoygen concentration sodium, its surface roughness showed only so slight an increase to 1.1 μm.

3.4 Changes in chemical compositions in the corroded surface

The typical results of X-ray microprobe dimensional analyses of the surface exposed to the low-oxygen concentration are shown in Photo 4. The analyses of each element were made at the same location.

The lights and shades in Photo 4 are in proportion to the concentrations of the elements, that is to say, the darker the shade, the lower the concentration. The white straight line (horizontal) is the place where the line analysis was made and the white zigzag line shows the analysis curve. Some correlation is observed between the shading in a photo and the line analysis curve. From these results, following relations are found. Ni and Cr have almost identical distribution, while Fe has an reverse distribution (tendency to Ni and Cr), that is to say that Fe increase where Ni and Cr decrease. The correlation between carbon and these elements is not revealed clearly from Photo 4. The surface has the regions of the maximum size of 10 μm with distinct decreases of Ni and Cr and a slight increase of Fe.

These regions coexist with the regions where the chemical compositions show a relatively small change. Photo (C) is a reflected electron beam image. From this photograph the correlation is not clearly observed between this image and the dimensional analysis image of the elements shown here. Fig. 10 shows the results of the line analysis of the specimen exposed to the high oxygen concentration sodium. The numerical values in this figure represent the element concentrations in the surface before and after sodium exposure, which were obtained by assuming that the line analysis level of the ground surface (the thickness of the surface layer removed by grinding: approx. 50 - 100 μm) is approximately the same value as the element concentrations before sodium exposure.[Note 3)] As in the case of the dimensional analyses in Photo 4, the line analyses showed the similar tendency that Fe increased while Ni and Cr decreased in the surface.[Note 4)]

Table 4 shows the mean values of elements (Fe, Ni, Cr) before and after sodium exposure and the maximum value of Fe and minimum values of Ni and Cr, obtained from Figs. 10 and 14 (plane, line analysis curve) in respect of the specimens in the surface exposed in the high and low oxygen concentration sodiums. This table indicates that the decreasing rates of Ni and Cr to the concentration of each element before exposure are about the same in high oxygen

---

Note 3): This assumption is based on the results of test in 3.6, i.e., the results of the characteristic X-ray analysis in the section showed that the chemical compositions indicated little change in the inner part more than about 30 μm from the surface after exposure to sodium.

Note 4): Since the positions of line analyses of the elements in Fig. 10 were slightly different, the correlations among these elements cannot be discussed from Fig. 10 alone. However, the XMA analyses made at the same position showed approximately the same results as Photo 4.

concentration sodium (Case-A), but the decreasing rate of Ni is remarkably higher than that of Cr in low oxygen concentration sodium (Case-B).

Fig. 11 shows the chemical compositions of the specimens as received and after 1,000 hrs sodium exposure (Case-A) plotted on the phase-equilibrium diagram[6] of the Fe-Ni-Cr system at 650 °C.

Table-4 Change in chemical composition due to sodium exposure

Material / Condition / Element	Check Analysis, Mean Value (As Received Material)	Xray Microprobe Analysis (As Exposed Material in Sodium at 650°C)			
		Case-A		Case-B	
		Mean Value	Max. or Min. Value	Mean Value	Max. or Min. Value
Fe	65.0	71.5	Max. 81.7	73	—
Cr	17.0	12.9	Min. 10.9	13	Min. 9.6
Ni	13.1	10.9	Min. 8.5	9	Min. 2.4

Case-A... 12ppm O_2 in sodium for 1000hr

Case-B... 5ppm O_2 in sodium for 2000hr

It is seen from this figure that the maximum shift position on the surface of specimen exposed to sodium is within the region where has the B.C.C. (body-centered cubic) and F.C.C. (face-centered cubic) structures coexist. It is supposed that the surface crystal structure of the specimen exposed to the high oxygen concentration sodium (650 °C, 1,500 hrs) is composed of two different structures, i.e., B.C.C. and F.C.C.

3.5 X-ray diffraction of corroded surface

Fig. 12 shows the diffraction patterns of the specimens as received and those exposed in high oxygen concentration sodium (650 ^{o}C, 1,000 hrs). The specimen as received had only the diffraction pattern from the F.C.C. structure (γ-iron). As predicted in 3.4, the sodium exposed specimen showed not only the F.C.C. diffraction pattern but also the (110) reflexion of α-iron, showing the B.C.C. patterns disappear when the sodium exposed surface layer is removed by grinding, they are considered to be the result of the phase transformation (refer to Fig. 11) due to the changes in the chemical compositions in the surface caused by the exposure to sodium. The specimen exposed to the low oxygen concentration sodium also showed the diffraction pattern of a higher peak value [α (110)] indicative of the presence of α grains and more distinct diffraction patterns [α(200) and (211)]. This may be understandable from the fact that both the mean shift and maximum shift points of the specimen exposed in low of oxygen concentration sodium are plotted in Fig. 11 to the left side compared with those of the specimen exposed to the high oxygen concentration sodium.

3.6 Changes in chemical compositions at the section of the specimen (in the neighborhood of the surface exposed in sodium)

Since the grain boundary diffusion coefficient is larger than the volume diffusion coefficient in the temperature range around 650 ^{o}C in the case of austenite stainless steel, the leaching and depletion of alloy elements are expected in the grain boundary in the nieghborhood of the sodium exposed surface layer. The X-ray microprobe scanning was mode at the sections of various depths in parallel to the

surface. Figures 13 and 14 show some of the results. The specimens exposed to high and low oxygen concentration sodium had a tendency that Ni and Cr were depleted locally and Fe increased in the same place. This is in agreement with the result of the dimensional analysis at the surface as shown in Photo 4. The amplitude of such local changes and the frequency of occurrence of such changes decrease in the inner part and almost no change occurs in the chemical composition at the depths more than 30 μm from the surface.

The X.M.A. of the specimen of which the grain boundary was revealed by etching slightly showed that such local changes of element concentrations occurred in the grain boundary. Figures 15 and 16 show the depletion and leaching of Fe, Cr and Ni in the neighborhood of the grain boundary in the direction of depth and the distribution of carbon in the matrix. From these figures, it is seen that the grain boundary depletion layer at the section in the neighborhood of the sodium exposed surface has a width of about 30 μm. Figures 15 and 16 show the changes in Fe, Ni and Cr concentrations, which are the mean values of the peak values (5 to 6 points) observed at the different depths from the surface. Almost no difference was observed in carbon concentration between the grain boundary and the matrix in the sectional direction but an increase presumably due to carburization was observed in the neighborhood of the surface.

The values plotted here are the X.M.A. analysis values of the matrix area.

3.7 Microstructure of specimens after sodium exposure

Photo 5 shows the microstructures in the longitudinal section of the cladding tube specimen before and after exposure in sodium. Any change in microstructure was not observed so distinct as to be expected from the results of the X-ray microprobe analyses but the grain boundary near the sodium exposed surface (photo 5, sectional microstructure, exposed to sodium for 2,000 hrs was observed to appear larger than that in the inner layer or in the neighborhood of the inner surface. Compared with the results of observations of the specimen as received, it is seen that the precipitation of carbide presumably due to temperature effects (effects of temperature maintained at 650 ^{o}C) occurs in the grain boundary and on the slip line and that the longitudinal strain marking produced in the tube drawing becomes less or disappears.

3.8 Changes of mechanical properties of sodium exposed specimens at room temperature

In order to investigate the influence of corrosion on the mechanical properties of the cladding tube, the tensile test was made at room temperature, using 1 mm wide ring-shaped test pieces. Figure 17 shows the results with the appearance of the test pieces. The strain in this figure is the ratio of the value of elongation and the gauge length. The gauge length was taken with the length of the external circumference of the test piece before testing. The stress is the nominal one. The photograph and stress-strain curve of the specimen after rupture evidently show remarkable decrease of yield stress and increase of elongation in the specimen exposed in sodium. The mechanical properties obtained from the stress-strain curve in

Fig. 17 were graphed in Fig. 18. This figure shows a slight decrease in tensile strength, and large decreases in yield stress and proportional limit, and an increase in elongation. Such changes in mechanical properties are presumably due to the effects of sodium exposure and temperature (the decrease of cold working effect due to temperature maintained at 650 ^{o}C, i.e., recovery and softening). A test to separate the effects of these two factors is under planning.

Photos 6 and 7 show fractographs of the ruptured surface and the microstructure of the ring tensile test specimen, respectively. The effect of corrosion on the rupture behavior does not appear distinctly. The upper side of the photo 6 is the sodium exposed surface of the specimen. The photomicrographs of tensile rupture specimens at room temperature do not show any signs of intercrystalline cracking.

4. Discussion

In making a discussion, we will first consider the surface corrosion behavior and then the internal corrosion in the grain boundary and in the matrix and finally the influence of corrosion on the mechanical properties.

4.1 Surface corrosion and decrease of tube thickness

4.1.1 Dissolution of alloying elements

Figure 19 shows the obtained reduction rates of tube wall thickness together with the data of A.W. Thorley[3] (straight lines). It is considered that the PNC data are not so much deviated from Thorley's lines in the various oxygen concentrations. As is evident from Figures 8 and 19 and the data of E.L. Zebroski,[4] the metal loss rate (reduction rate of tube wall thickness) calculated from the overall weight change is greatly influenced by oxygen concentrations in sodium. It is considered because the oxygen concentration in the neighbor of the metal surface in contact with sodium determines the dissolution rate of alloying elements from the metal surface. However, paying attention to one of the important constituent elements, e.g., Ni, it is seen that the specimen exposed to the low oxygen concentration sodium shows a greater metal loss than that exposed to the high oxygen concentration sodium as seen from Table 4.
The rates of loss of some elements do not necessarily depend on the oxygen concentration in sodium, that is to say, it is considered that the alloying elements do not have the equal degrees of dependence on oxygen concentrations for their corrosion. This resembles the results of the experiments of A.W. Thorley,[3] et al., that the rate of loss of Ni based alloy does not depend on the oxygen

concentration and what is stated by G.P. Wozadlo,[7] et al., about the oxygen concentration dependence of Ni, Cr and Fe, the main constituents of stainless steel. As they have stated about the dissolution of Ni from a Ni-based alloy, it may be considered that the dissolution of Ni from Type-316 SS is not the dissolution in the form of oxide but atomic dissolution. If the dissolution. If the dissolution of Ni, which is one of the main elements (Fe, Cr, Ni) constituting Type-316 SS cladding tube specimen should not depend on the oxygen concentration or its dependence on the oxygen concentration is very small, since the total amount of dissolution obtained as the weight loss has a distinct dependence on the oxygen concentration, the dissolution of the other elements, i.e., Fe and Cr or either of them are presumed to have a distinct dependence on on the oxygen concentration. The data obtained here alone are not sufficient to experimentally prove this presumption.

4.1.2 The influence of the tube thickness decrease and the surface roughness change on pressure drop of flowing sodium

The surface roughness of the cladding tube changes due to the corrosion by sodium. Since the surface roughness change is presumed to affect the drag coefficient of a fluid and the pressure loss, we tried to calculate the amount of pressure loss versus the change of surface roughness in the M-2 loop test (1,000 hrs, 650 °C) by means of Colebrook and White's formula.[Note 5] We substituted the e/d value before and after the test in this formula and plotted the

---

Note 5): Colebrook and White's formula, $1/\sqrt{\lambda} = -2\log\left(\frac{e/d}{3.17} + \frac{2.51}{Re \cdot \sqrt{\lambda}}\right)$

λ : draw coefficient e: surface roughness

d : equivalent diameter

Re($=\frac{v.d}{}$): Reynolds number v : flow velocity

: coefficient of kinetic viscosity

relation between the Re number and λ to obtain a graph as shown in Fig. 20. The Re number of M-2 loop becomes 1.39×10^4. Here we used the following values in the calculation of the Re number. $v = 2.6$ m/sec, $d = 1.3$ mm, $\gamma = 2.43 \times 10^{-7}$/sec (650 °C). Therefore, from the figure, λ before and after the test becomes 0.0292 and 0.0298 and the increase of pressure loss[Note 6] before and after the test becomes 2%.

Next, we calculated the pressure loss by applying the surface roughness change obtained by this test to the "JOYO" conditions. In the case of "JOYO" conditions, Colebrook and White's formula can be plotted as shown in Fig. 21. By making a similar calculation, the Re number ($v = 5$ m/sec, $d = 3.15$ mm, 2.85×10^{-2} m^2/sec...510 °C) becomes 5.53×10^4. From Fig. 21, λ before and after the test becomes 0.0216 and 0.0222 and the increase of pressure loss about 3%.

The data of surface roughness used in this calculation were those obtained by the test on the specimen exposed to sodium for 1,000 hours, and the surface roughness is relatively small. However, when the specimen is exposed to sodium for a longer time, the surface roughness will increase and the pressure loss will also increase as the test proceeds, thus causing possibility that a specified flow rate of sodium cannot be obtained. In Figure 21 is plotted the relation between the Re number and λ when the surface roughness is 5 μm (a typical example for the calculation of the conceivable surface roughness change). In this case, λ becomes 0.0252 when

---

Note 6): As for the value of surface roughness to be substituted in the calculation formula, we used a three-digit value (mean value for three regions) for the convenience of calculating process.

the Re number is 5.526×10^4 and a 17% increase of pressure loss is predicted after the test. From what has so far been discussed, in the actual reactor there is the possibility of an insufficient pump head in the extreme case and a decrease in the flow rate and in some cases the overheating and melting of the fuel pins. So, it is considered necessary to make measurements of pressure loss during test.

4.2 Internal corrosion

4.2.1 Intergranular corrosion

As shown in Figures 15 and 16, the depletion of Ni and Cr and the leaching of Fe occur in the grain boundary at a depth less than about 30 μm from the sodium exposed surface. Previously, a weakening tendency of the intergranular bond has been observed in this depletion layer. For instance, we have a case in which a shallow intergranular cracking developed in the tensile test of Type-316 SS at room temperature and 650 °C after exposure to 650 °C sodium[8] and a case in which a shallow intergranular cracking was observed in the 180 ° bending test of Type-304 SS at room temperature after exposure to 600 °C sodium.[9] As for an other example of observation of intergranular corrosion in a longer duration of test, there is a case in which an intergranular corrosion as deep as 0.18 mm was observed at a G.E. loop,[4] in which the corrosion was observed in the piping at the boundary between the temperature rising section and the temperature lowering section after a 30,000 hrs test in sodium of 650 °C at maximum. G.E. says that such intergranular corrosion depended on the oxygen concentration in sodium and the stress level.

Photo 8 shows the scanning electron micrographs (SEM) of the outer surface in the neighborhood of fracture after ring tensile test of the specimen exposed to sodium. From these scanning electron micrographs, no intergranular cracking was observed in the neighborhood of fracture. Although shallow intergranular cracking was observed locally only in the outer surface of the specimen exposed to the low-oxygen concentration sodium as shown in Photo 8, it is difficult to definitely ascribe it to corrosion by sodium. The fracture morphology in the neighborhood of the sodium exposed surface shows the ductile rupture showing dimple patterns (Photo 6). From the results of the present test and reference literatures (4), (8) and (9), it is presumably due to the depletion of Ni, Cr and leaching of Fe in grain boundary that the decrease of bond of grain boundary is so much more than that of bond of matrix as to cause intergranular cracking in the corroded surface layer in the tensile or bending test at room temperature. In these reference literature, since the oxygen concentrations are relatively high, the appearance of shallow intergranular cracking in the specimens exposed to sodium (after tensile or bending test) suggests the possibility of decrease of Cr in the grain boundary. In addition, from the facts that the intergranular slip is more apt to occur in the tensile test and the like test at high temperature than at room temperature and that the phenomena of leaching and depletion in the grain boundary near the sodium exposed surface will have a tendency to further decrease the intergranular bond, it is presumed that shallow intergranular cracking is apt to occur in the corroded surface layer.

The important subject about the intergranular corrosion is probably whether it is progressive or not, that is, whether the depletion

of Ni and Cr and leaching of Fe will progress into the deeper layer of the tube as exposure time is longer. We have a report[10] which says that the depletion layer does not progress more than a certain thickness. However, much more studies and experiments will be needed to verify these considerations.

4.2.2 Shift of alloying elements in the internal matrix

Figs. 15 and 16 show the concentration distributions of carbon as well as Fe, Cr and Ni obtained by XMA analysis at various depths from the sodium exposed surface. In the case of carbon, unlike the behavior in the grain boundary of the substitution-type elements such as Fe, Ni orCr, there is no difference in its distribution in the grain boundary and in the grain (this is presumably because carbon is an interstitial-type element) and it was observed increasing, an increase of carbon, that is, carburization, was observed from a depth of about 30 μm.

As seen from Fig. 22, nitrogen also showed a slight increase, although not so distinct as in the case of carbon, in the neighborhood of the surface. The increase of nitrogen is presumably due to the penetration of nitrogen contained in the cover gas (argon gas) through sodium but it is unknown what route it takes to penetrate. A further study must be made on this problem from the viewpoint of the production of He and the decrease of high-temperature strength due to N (n, α) reaction caused by the fast neutrons when used in the reactor and of the deterioration of material properties by nitriding.

The depletion or leaching of Fe, Ni and Cr in the matrix except the neighborhood of the grain boundary was within about 5 μm - 10 μm in the present experiments. In the experiments in the

temperature range below 2/3 Tm,[Note 7] D_S (surface diffusion coefficient) > D_G (grain boundary diffusion coefficient) > D_L (lattice diffusion coefficient) and the grain boundary diffusion takes an important proportion of the entire diffusion.[11] Considering the fact that the phenomena of depletion and leaching of these substitution-type elements depend on the diffusion in the matrix in the neighborhood of the grain boundary, the evaluation of corrded layer of grain boundary is considered sufficient when the problem is the internal corroded layer in the FBR cladding tube (Type-316 SS) which is used at temperatures lower than 700 °C in the actual reactor.

4.3 The influence of the corrosion in sodium on the material strength

The corroding effects in the monometallic loop are considered to be produced chiefly by the following material and working conditions.

The factors influencing corrosion in sodium

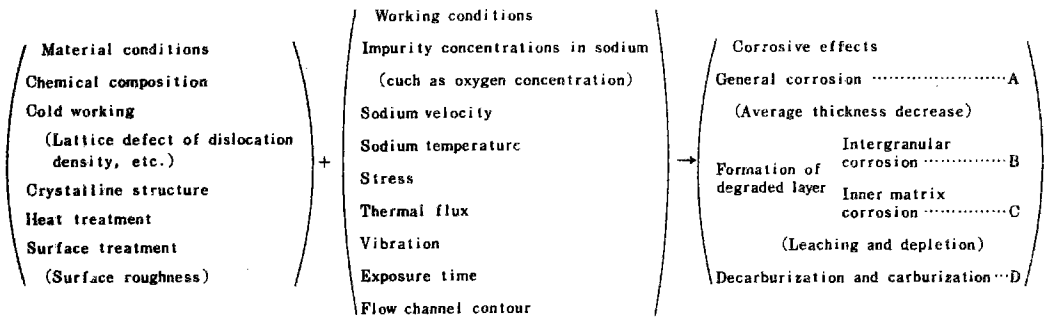

With regard to the degree of influence of general corrosion on the material strength of the cladding tube, simple calculations[Note 8] are made to make a comparative study of the effects of oxygen concentrations and the following results (the reduction of material strength

---

Note 7): Tm is the melting point on the absolute temperature scale. For instance, 2/3 Tm in the case of 316 SS is 1,113 °K ~ 1,096 °K (840 °C ~ 823 °C).

Note 8): A simple evaluation of material strength reduction due to exposure to sodium.

(a) Rate of decrease of tensile rupture load or yield load $K_1 = 1 - \frac{W_t}{W_o}$

$W_o = \frac{\pi}{4}(D_o^2 - D_i^2)\sigma_B$ (or σ_y) ..... Tensile rupture load before exposure to sodium (yield load)

$W_t = \frac{\pi}{4}(D_t^2 - D_i^2)\sigma_B$ (or σ_y) ..... Tensile rupture load after exposure to sodium

(b) Short-time internal pressure rupture strength $K_2 = 1 - \frac{P_t}{P_o}$

$P_o = \frac{D_o^2 - D_i^2}{D_o^2 - D_i^2} \cdot \sigma_{Bh}$ ..... Internal pressure rupture strength before exposure to sodium

$P_t = \frac{D_t^2 - D_i^2}{D_t^2 - D_i^2} \cdot \sigma_{Bh}$ ..... Internal pressure rupture strength after exposure to sodium

(c) Rate of decrease of creep rupture life $K_3 = 1 - \frac{t_{rt}}{t_{ro}}$

$t_r = \left(\frac{C}{\sigma_o}\right)^n$ ..... Creep rupture life before exposure to sodium

$t_{rt} = \left(\frac{C}{\sigma_o \frac{D_t^2 - D_i^2}{D_o^2 - D_i^2}}\right)^n$ ..... Creep rupture life after exposure to sodium

where $D_o = 6.3\,mm$ ..... outside diameter before exposure to sodium

$D_i = 5.6\,mm$ ..... inside diameter before exposure to sodium

$D_t = \begin{cases} (6.3-0.034)\,mm \\ (6.3-0.004)\,mm \end{cases}$ outside diameter after exposure to sodium

σ_B = tensile rupture strength

σ_y = yield strength

σ_{Bh} = short-time internal pressure rupture strength (maximum hoop stress)

$C = 41$

$n = 7$ ..... creep constant

As for the values of C and n which are used here, we used the estimated values deribed from the data obtained by the creep rupture test (12 ppm O_2) of the cladding tubes from the same lot in 650 °C sodium.

of the cladding tube after a year of use in sodium). In both cases of A and B, the calculations are made from the maximum value of the thickness change rate as shown in Appendix 2.

Reduction of material strength after 1-year use in sodium

(in the calculations are used the maximum values in the data of 1,000 hr test) (see Appendix 2)

		A	B
(a)	Tensile rupture load or yield load	0.7% decrease	8% decrease
(b)	Short-time rupture internal pressure strength	0.5% decrease	5% decrease
(c)	Creep rupture life	6% decrease	30% decrease

A: Low-oxygen concentration sodium exposure (cold trap temperature 150 °C, 5 ppm O_2)

B: High-oxygen concentration sodium exposure (cold trap temperature 200 °C, 12 ppm O_2)

This is a simple evaluation which has been made without taking into consideration the effects of the degraded layer, and decarburization and carburization. From the above results, it is considered necessary for the oxygen concentration in sodium to keep below about 10 ppm O_2 for a cladding tube with a thickness of about 0.35 mm. With regard to the influence of exposure in sodium on the actual material strength, we investigated only the mechanical properties by the ring tensile test and the exposure time was so short that the results shown in Figure 18 cannot be directly corresponded to the above values of the material strength change. The results shown in Figure 18 can be interpreted as follows. The sodium exposed surface showed the decrease of

material strength and the increase of ductility, which were contradictory to the expected effects of carburization (i.e., an increase of material strength and a decrease of ductility and expected due to this degree of carburization). This is probably because the effect of 10% cold working decreased due to the maintenance of temperature at 650 ^{o}C, thus offsetting the effect of carburization. From the results of the present experiment, it is impossible to make a quantitative evaluation of the effect of corrosion and that of the maintenance of temperature at a constant level separately. As for this question, we have to wait for the results of experiments to be made in the future.

5. Conclusions

The following conclusions can be drawn from the results of the above test of the domestically produced FBR fuel cladding tube in flowing sodium.

(1) Dependence of general corrosion on the oxygen concentration in sodium:

At 650 °C distinct differences were observed in the change of weight, i.e., the decrease of thickness, as a result of the metal loss, according to different concentrations of oxygen in sodium (Figure 8). The thickness decrease became larger as the oxygen concentration increase. Such being the case, it is desirable to maintain the oxygen concentration in sodium at around 10 ppm or at a higher degree of purity when AISI Type-316 cladding tube is actually used.

(2) Intergranular corrosion:

In addition to the decrease of thickness accompanying the weight change, a layer in which there occurred the depletion of Ni and Cr and leaching of Fe (Figures 13 and 14) was observed extending about 30 μm inward along the grain boundary (Figures 15 and 16). Such being the case, a further study is needed to make investigations on the changes taking place in such depletion layers with respect to time and the effects of the formation of such layers on the mechanical properties of the cladding tube. Since the depletion layers in the internal matrix are shallow as compared with those in the grain boundary, it is necessary for the evaluation of the depletion layer to be made on the depletion layer in the grain boundary.

(3) Production of ferrite (α phase):

Fundamental findings have been obtained with regard to the formation of grains of ferrite (α phase)(Photo 4, Figure 12), surface corrosion (Photo 3), increase of surface roughness (Figure 9),

and changes in mechanical properties at room temperature (Figures 17 and 18).

Postscript

This experimental study was made as a part of the research and development project on the FBR fuel cladding tube to be used in sodium. Since this is an interim report before the ultimate goal is achieved, it is not perfectly satisfactory. However, we have carried out our experiments on the cladding tube itself and some of the tests were conducted under severe working conditions and therefore the qualitative data thus obtained for the corrosion behavior will useful in the development of the cladding tubes for "JOYO", "MONJU" and other reactors to be used in the future. We would like to carry out further experiments of longer durations at higher temperatures in an attempt to accumulate data and improve their reliability so that such data may be useful in designing FBR fuel assemblies and in the evaluation of their dependability.

References

(1) Yuhara, et al.: Technical Report on Material Test in Sodium (2), Mass Transfer and Fretting Corrosion Test of FBR Fuel Cladding Tube, PNC unofficial report (1972)

(2) V.J. Rutkauskas: LA-387 (1968)

(3) A.W. Thorley, et al.: Alkali Metal Coolant, SM-85/18, IAEA, Vienna (1967)

(4) E.L. Zerbroski, et al.: Alkali Metal Coolant, SM-85/28, IAEA, Vienna (1967)

(5) H.U. Borgstedt, et al.: KFK-991 (1969)

(6) ASTM: Symposium on the Nature, Occurrence, and Effects of Sigma Phase (STP No. 110), (1951)

(7) G.P. Wozadlo and C.N. Spalaris: GEAP-13544 (1969)

(8) Yuhara, et al.: Pre-print of Annual Meeting, the Atomic Energy Society of Japan, D-9 (1969)

(9) Japan Welding Society, Report on Experimental Study (2) accompanying the Sodium Exposure Test of FBR materials (Research work done at the request of PNC, 1972)

(10) J.N. Anno and J.A. Walowit: Analysis of corrosion of Stainless Steel in a Sodium and High Radiation Environment, Nuclear Technology Vol. 10, January (1971)

(11) W. Hume-Rothery: The Structures of Alloys of Iron; An Elementary Introduction, Pergamon Press, Ltd. (1966).

(12) Yuhara, et al.: Technical Report on Material Test in Sodium (1), Creep Test of FBR Fuel Classing Tube, PNC unofficial report (1971)

Appendix 1 Results of chemical analyses of impurities in sodium

(i) Sodium analysis at high oxygen concentration

The values given here are the results of the analysis carried by Takani and other research staff of the Analysis Laboratory of the Sodium Technology Development Section. The 1,000 hr test was carried out at M-2 as a part of the 2,500 hr test at the low-purity material loop.

The values of impurities present in sodium during the 2,500 hr operation of the low-purity material test loop

1st analysis : Cold trap temperature 185℃
2nd analysis : Cold trap temperature 258℃
Unit (ppm)

Element	1st specimen	2nd specimen	Remarks
Cr	0.54, 0.65 } < 1	0.39, 0.62 } < 1.	Absorption photometry
Fe	0.66, 0.66 } < 1	1.18, 1.18 } ~1	〃
Ni	0.20, 0.37 } < 1	0.24, 0.32 } < 1	〃
Mo	0.71, 1.78 } ~ 1	2.00, 2.24 } 2	〃
C	8.1, 5.6, 3.9 } Mean Value 5.9	9.6, 11.3 } Mean Value 10.5	Wet manometry method
O	10.8, 6.0, 9.0 Mean Value 8.6	20.8, 22.0, 26.7 24.2 26.8 Mean Value 24.1	Mercury amalgam method

Since the cold trap temperature was set at 200 °C in the low-purity material loop in the 2,500 hr and 1,000 hr tests, the oxygen concentration during the operation of the loop is obtained from the above values by simple proportional calculation by use of interpolation to be 12 ppm.

During the 2,500 hr continuous operation of the loop, the plug temperature was being measured by means of the plug meter attached to the loop. With cooling rate of (3 ±1) °C/min at the plug meter, the plug temperatures near the cold trap temperature at the time of sampling were as follows (mean values of the four experimental values).

Cold trap temperature	Plug temperature	Remarks
256	226 °C	Scattering of measured temperatures was less than ±3 °C.
172	147 °C	

We are now studying the correlation between these results of the plug meter test and the results of chemical analysis.

(ii) Sodium analysis at low oxygen concentration

Oxygen concentrations in sodium in medium-purity material test loop

Cold trap temperature	150 °C
Sampling method	Metallic vacuum tube method
Method analysis	Mercury amalgamation method
Analytical value of oxygen (ppm)	5.0, 6.8, 3.9, 6.2 mean value 5.5

Appendix 2 Data of weight changes of FBR fuel cladding tube (Type-316 SS)

(i) M-2 loop test (high oxygen concentration, about 1,000 hrs)

Specimen A 6.3ϕ (O.D.) x 100 mm (L) ...including welded end plugs

Item / Test section	Weight before sodium exposure (g)	Weight change after sodium exposure (g)	Weight change (g)	Thickness Change per year (Micron/year)	Tube symbol
T-1 (~650℃)	1350282	1348362	−001920	−11.1	S
T-2 (~440℃)	1246711	1347212	+000501	+ 2.9	〃
T-3 (~390℃)	1350376	1350480	+000104	+ 0.6	〃
T-4 (~300℃)	1350557	—	—	—	〃
T-5 (~370℃)	1345962	—	—	—	〃

Specimen B 6.3ϕ (O.D.) x 150 mm (L)

Item / Test section	Weight before sodium exposure (g)	Weight change after sodium exposure (g)	Weight change (g)	Thickness change per year (Micron/year)	Tube symbol
T-1 (~650℃)	7.86755	7.77910	−0.08845	−34.1	S
T-2 (~440℃)	7.86748	7.87669	+0.00921	+ 3.6	〃
T-3 (~390℃)	7.87015	7.87309	+0.00294	+ 1.1	〃
T-4 (~300℃)	7.86571	—		—	〃
T-5 (~370℃)	7.86795	7.86875	+0.00083	+0.3	〃

Note: Specimens A and B of T-4 were pulled out about 100 hours after the commencement of the test because the pressure loss in the daughter loop increased so much that it became impossible to maintain the rated flowing conditions and thereafter the dummy holder was inserted. As for specimen A of T-5, its post-exposure weight data are omitted because it suffered scratches when pulled out or washed.

(ii) M-II loop test (low oxygen concentration, about 2,000 hrs)

Specimen A 6.3φ (O.D.) x 100 mm(L) ... including welded end plugs

Item / Test section	Weight before sodium exposure (g)	Weight after sodium exposure (g)	Weight change (g)	Thickness change per year (Micron/year)	Exposure time	Tube symbol	Remarks
T − 1 (650℃)	10.61907	10.61302	−0.00605	−3.7	904	S−1466	
T − 4 (390℃)	10.62883	10.62919	+0.00036	+0.2	904	〃	
T − 1 (650℃)	10.61907	10.60877	−0.01030	−2.8	2062	〃	
T − 4 (390℃)	10.62883	10.62962	+0.00079	+0.2	2062	〃	

Specimen B 6.3φ (O.D.) x 150 mm(L)

Item / Test section	Weight before sodium exposure (g)	Weight after sodium exposure (g)	Weight change (g)	Thickness change per year (Micron/year)	Exposure time	Tube symbol	Remarks
T− 1 (650℃)	7.85946	7.85198	−0.00748	−3.0	904	S−3718	
T − 4 (390℃)	7.85872	7.85922	+0.00050	+0.2	904	〃	
T − 1 (650℃)	7.85946	7.84604	−0.01339	−2.4	2062	〃	
T − 4 (390℃)	7.85872	7.85976	+0.00104	+0.2	2062	〃	

Note: In considering the actual use of the corrosion behavior of the cladding tube being limited only to the hot leg section, the importance of the highest temperature test section and also the pressure loss of the test loop itself, etc., the specimen were inserted into T-1 and T-4 only.

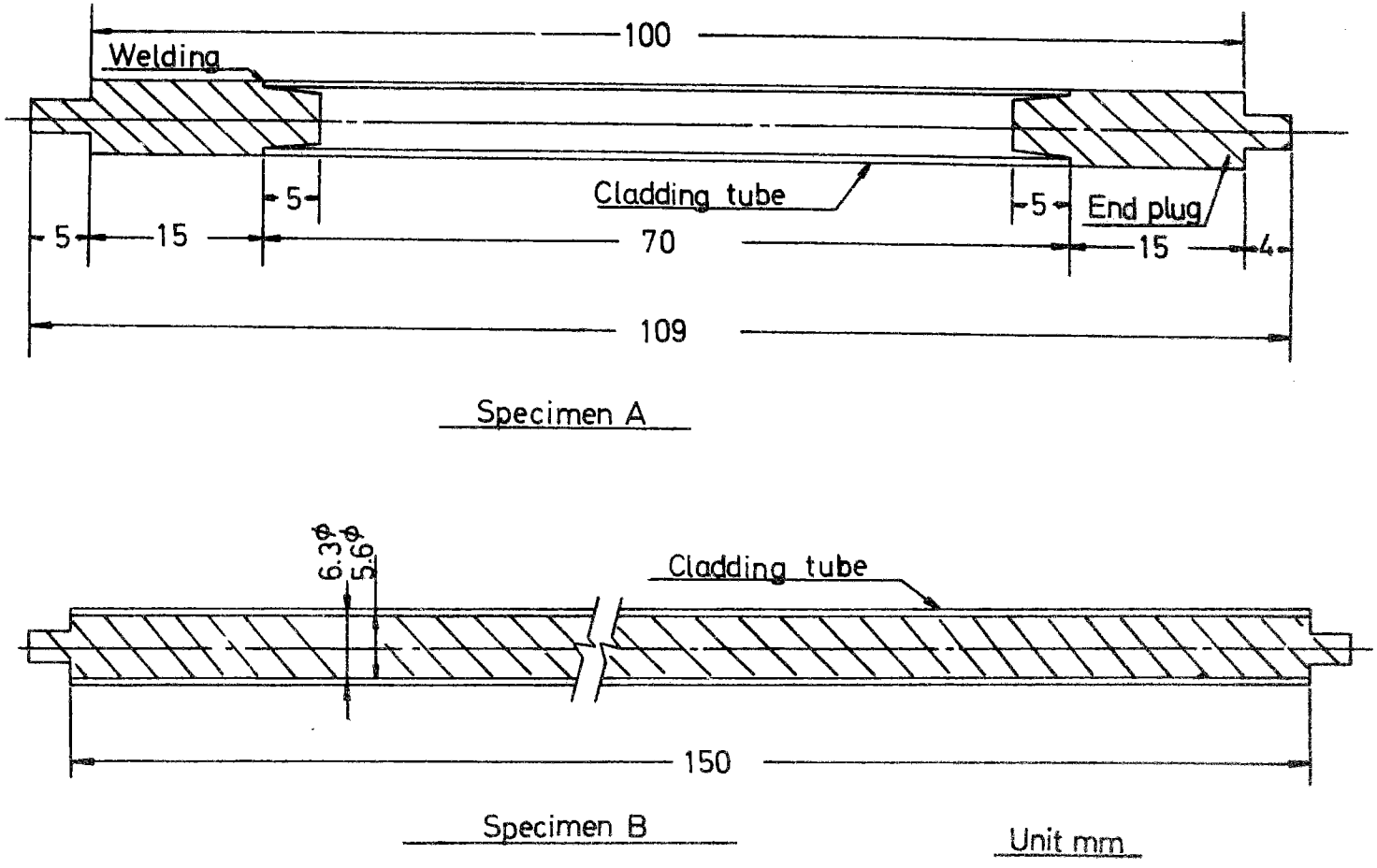

Fig. 1 Mass-transfer specimen figure of Type-316 stainless steel cladding tube.

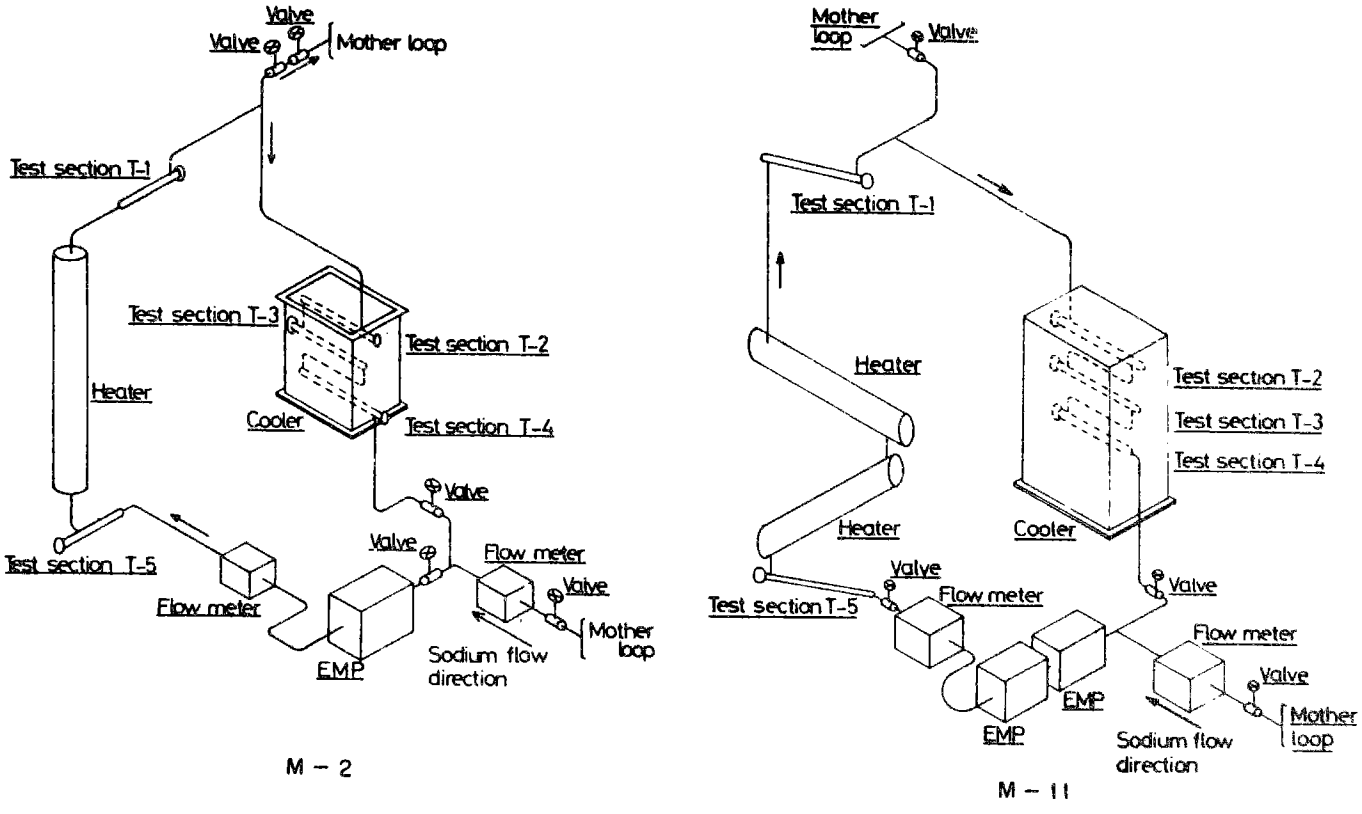

Fig. 2 Flow sheet of daughter loops for mass-transfer test (cladding tube specimen).

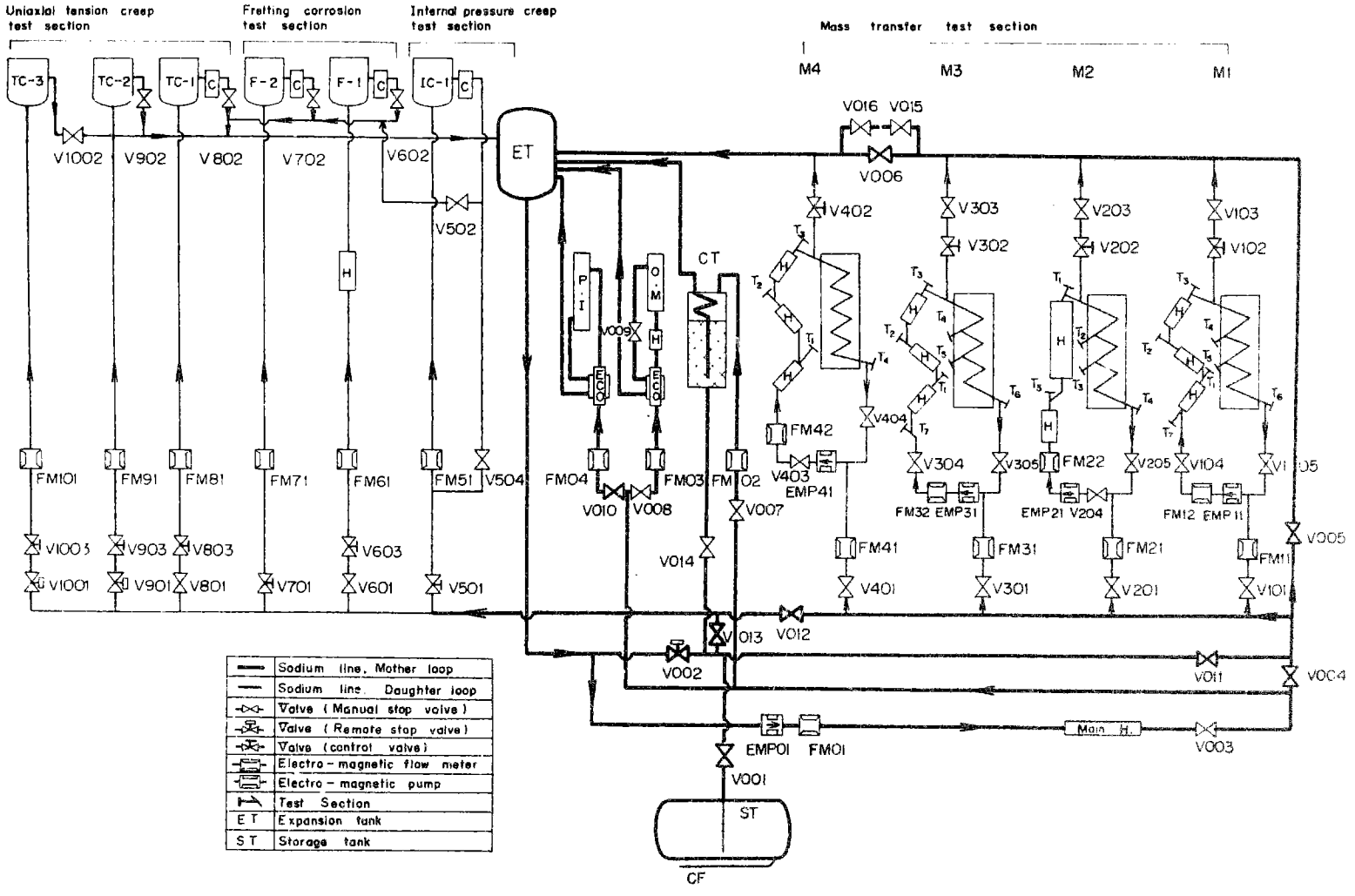

Fig. 3. Low-Purity Material Test Loop flow sheet.

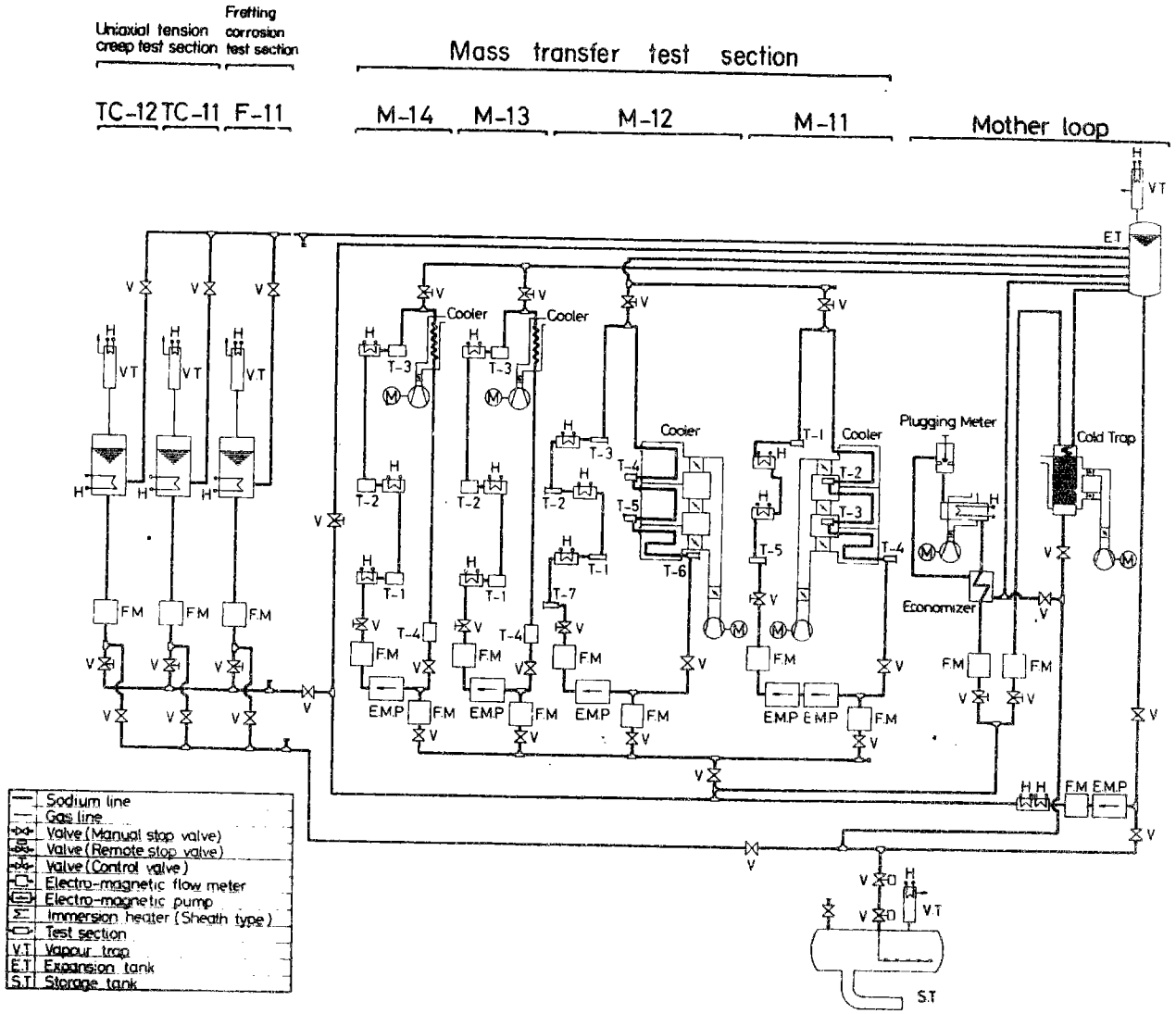

Fig.4. Medium-Purity Material Test Loop flow sheet.

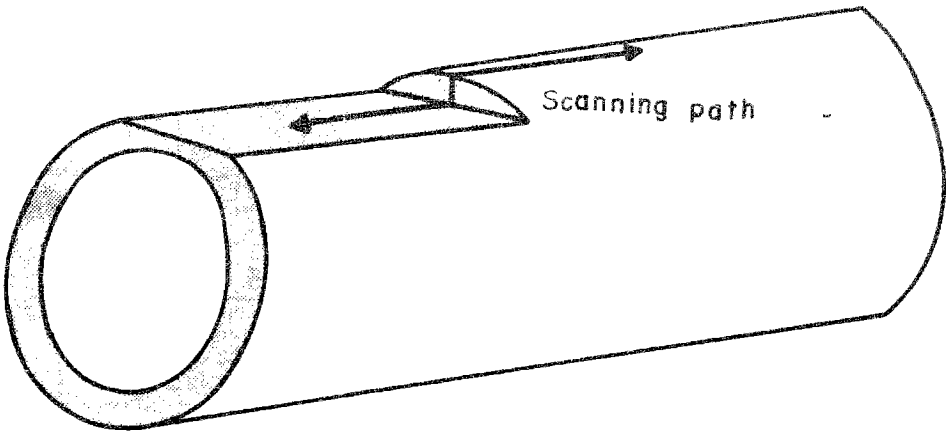

Fig.5. Schematic figure of the specimen for surface analysis due to Xray microprobe.

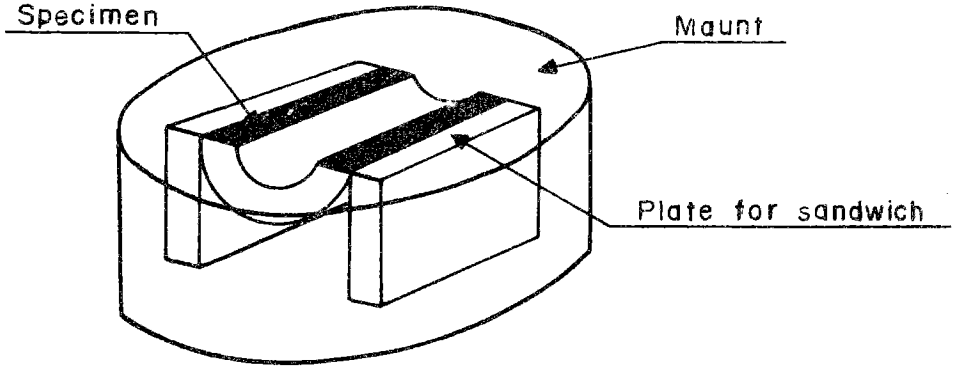

Fig.6. Specimen for Xray microprobe analysis of inner section.

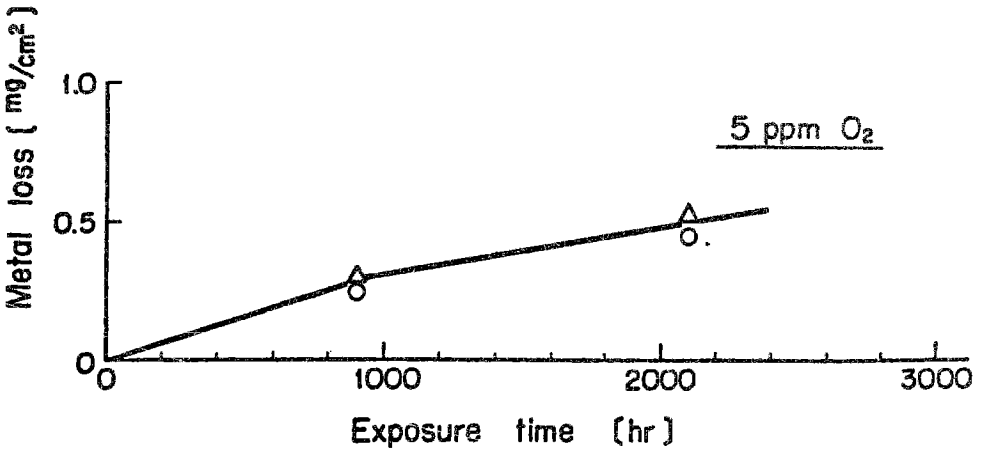

Fig.7. Metal loss of Type-316 cladding tube specimen in 650°C sodium.

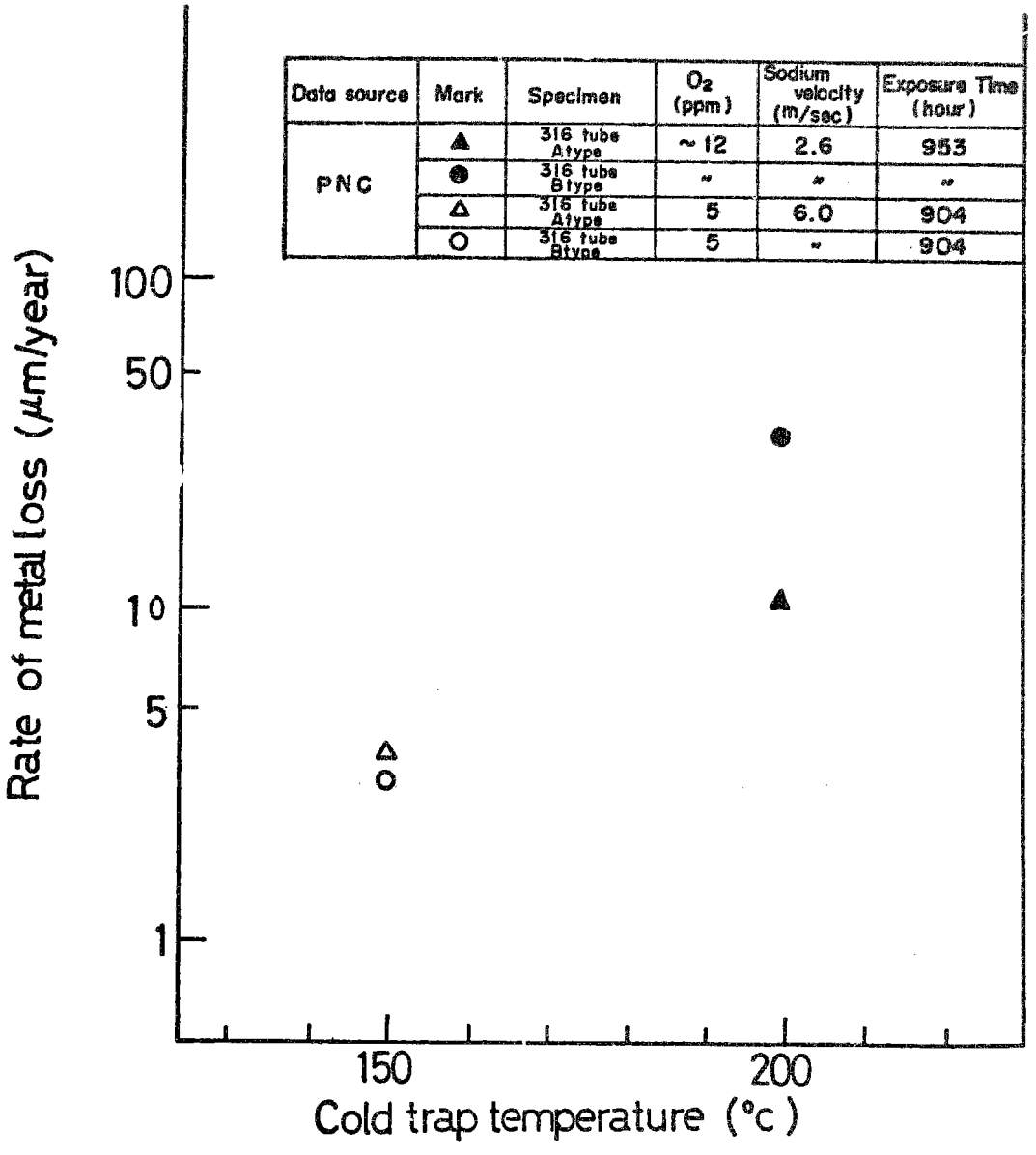

Fig. 8 Metal-loss rate of Type-316 cladding tube specimen versus cold trap temperature (in flowing sodium at 650°C).

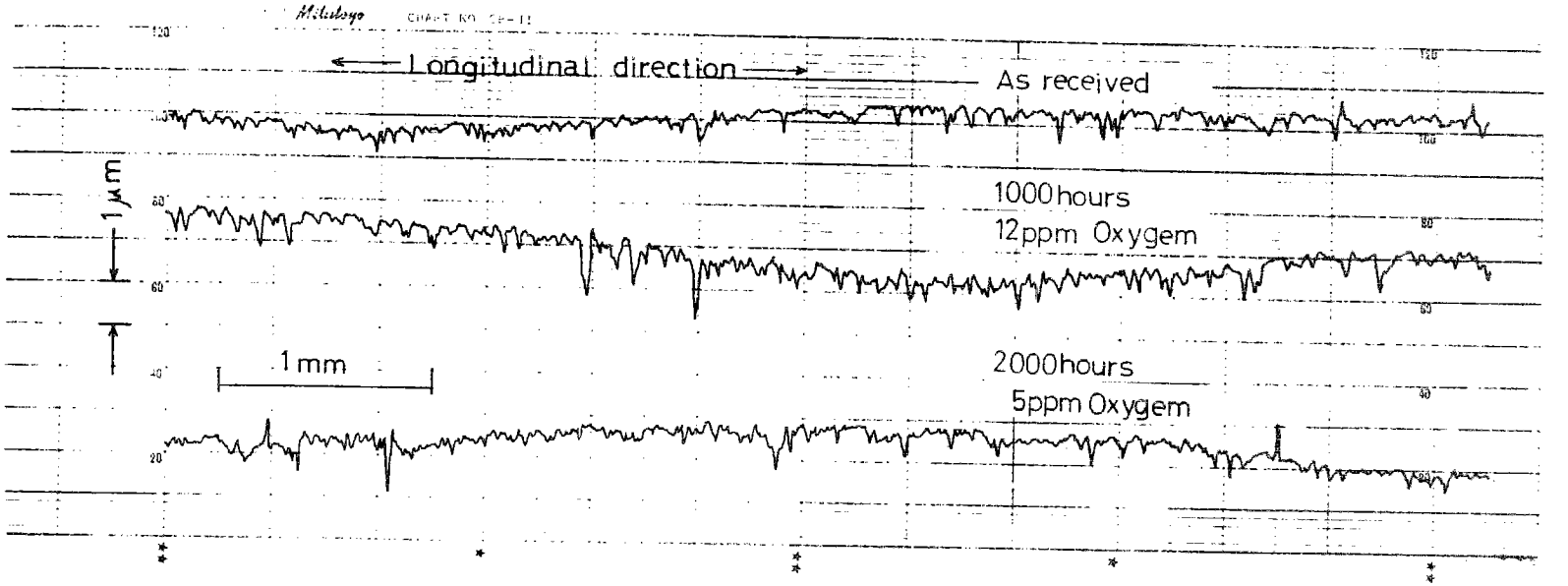

Fig. 9 Surface-roughness change of Type-316 stainless steel cladding tube specimen exposed in flowing sodium at 650°C.

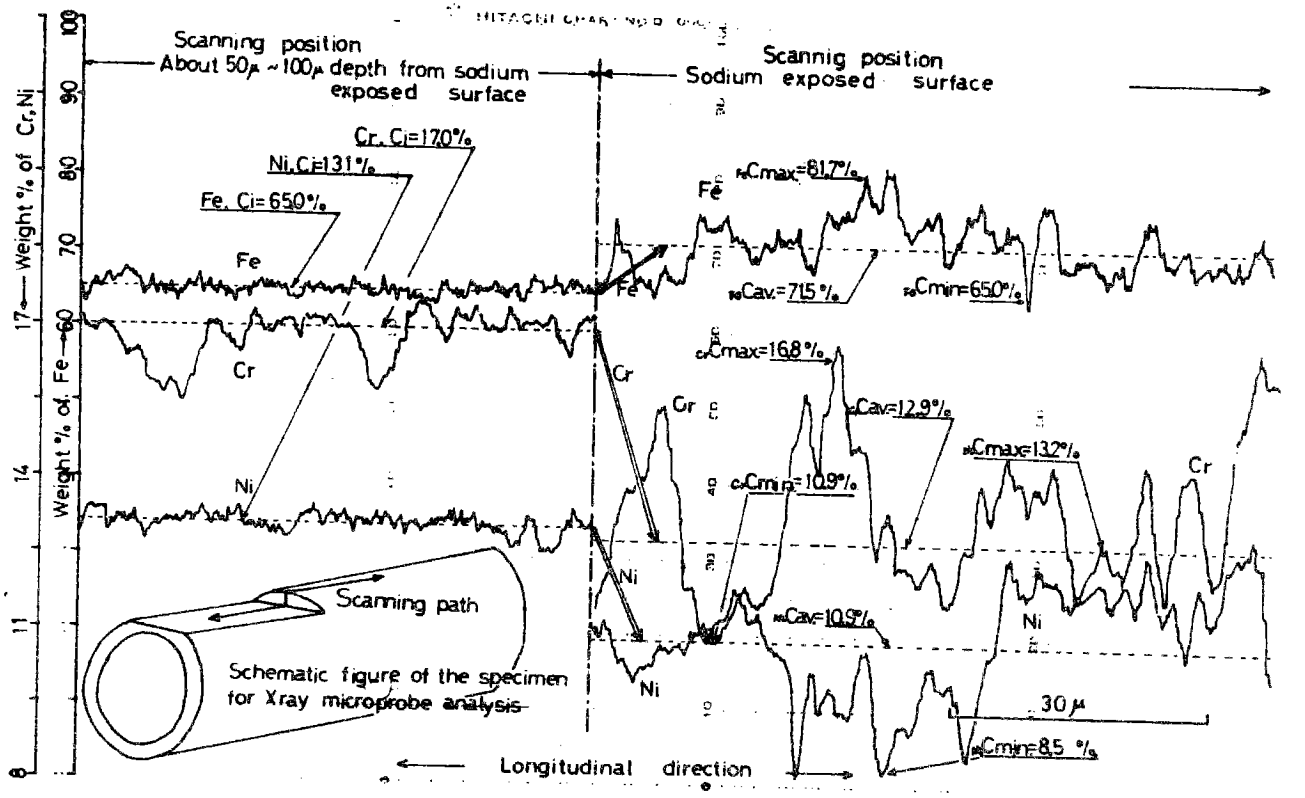

Fig.10. Xray microprobe analysis of Type-316 stainless steel cladding tube specimen exposed in flowing sodium at 650°C for 1000 hours.

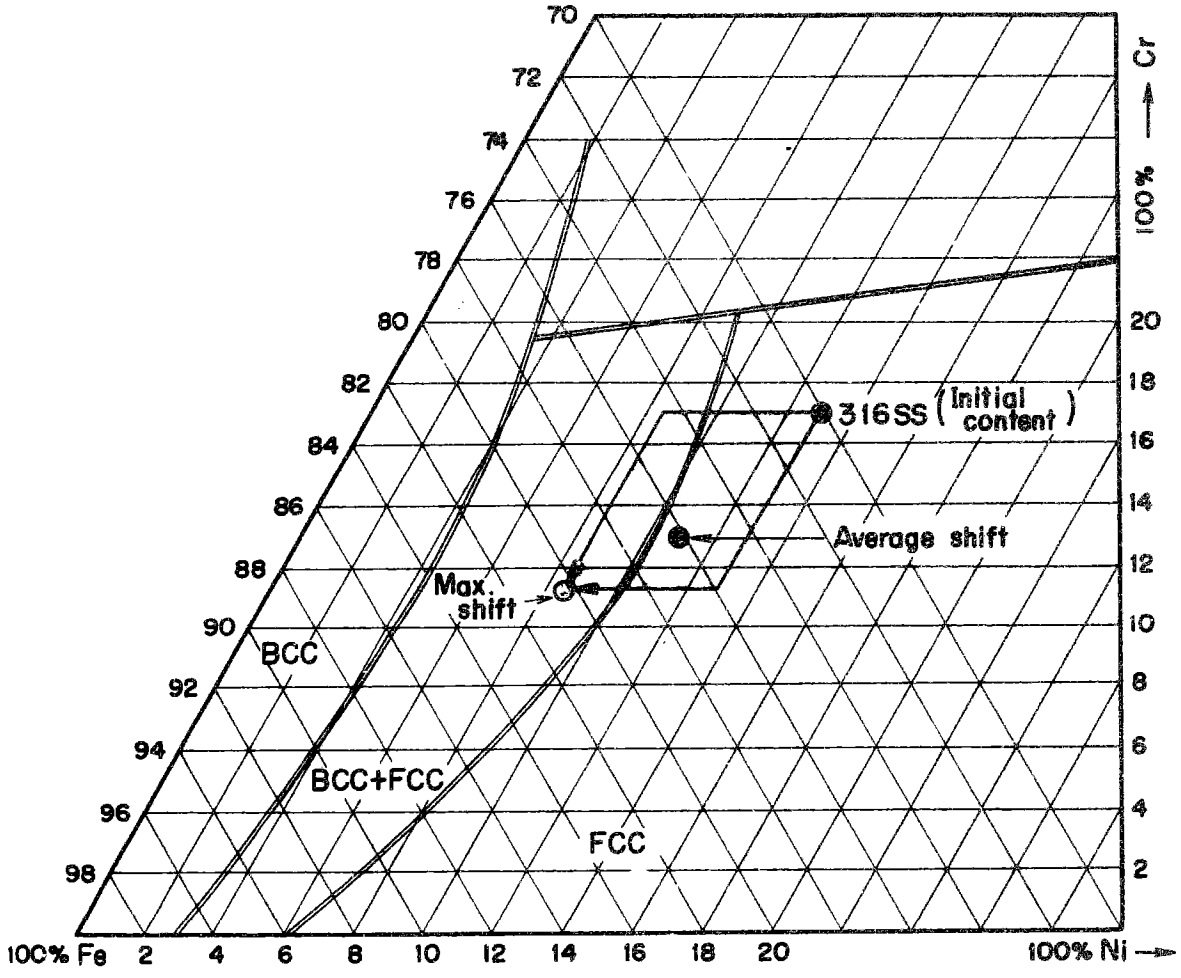

Fig.11. Approximate shift (from fcc to bcc phase) obtained by alloy composition change after sodium exposure.

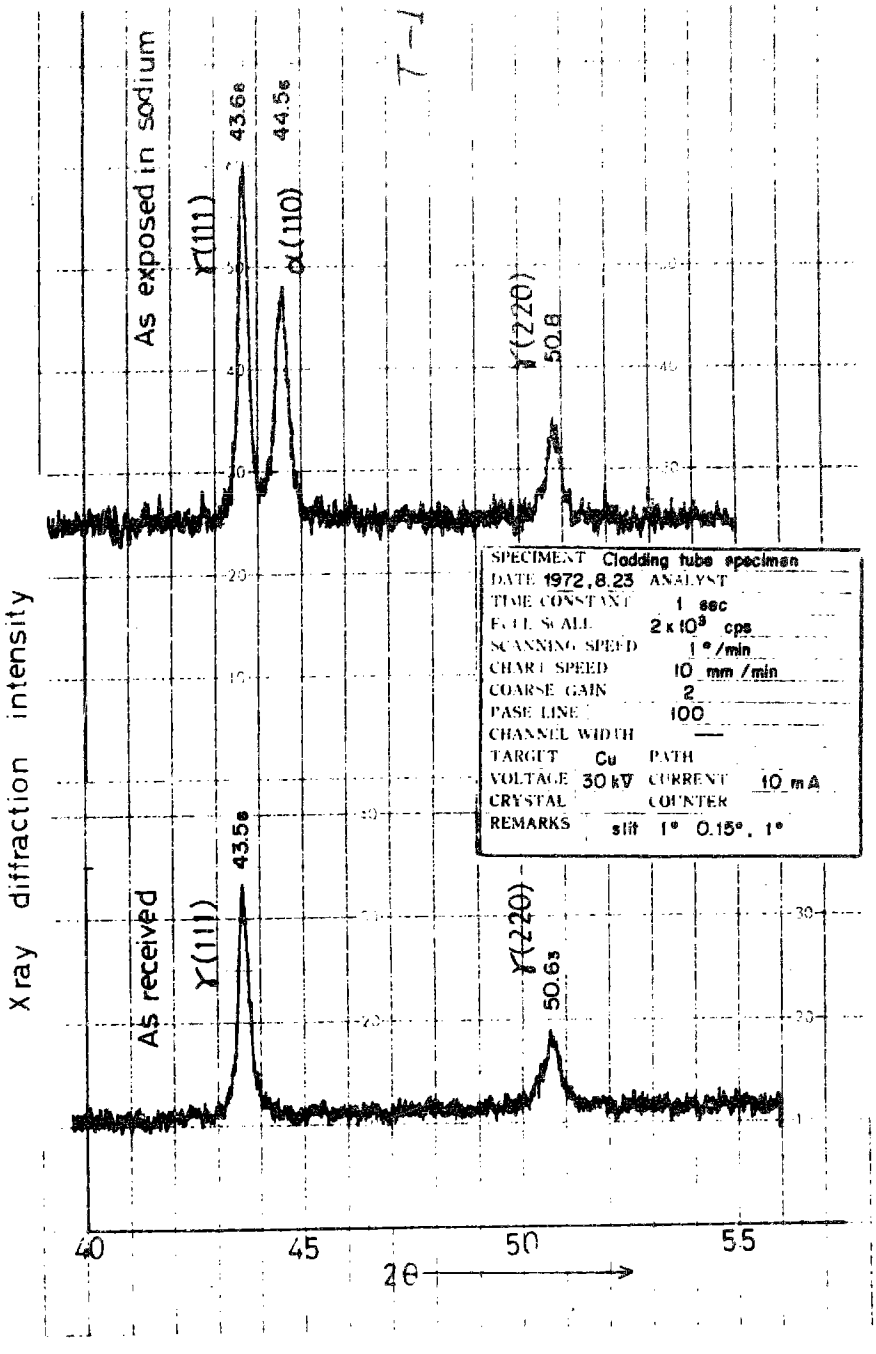

Fig.12. Phase shift observation from fcc to bcc by Xray diffraction.

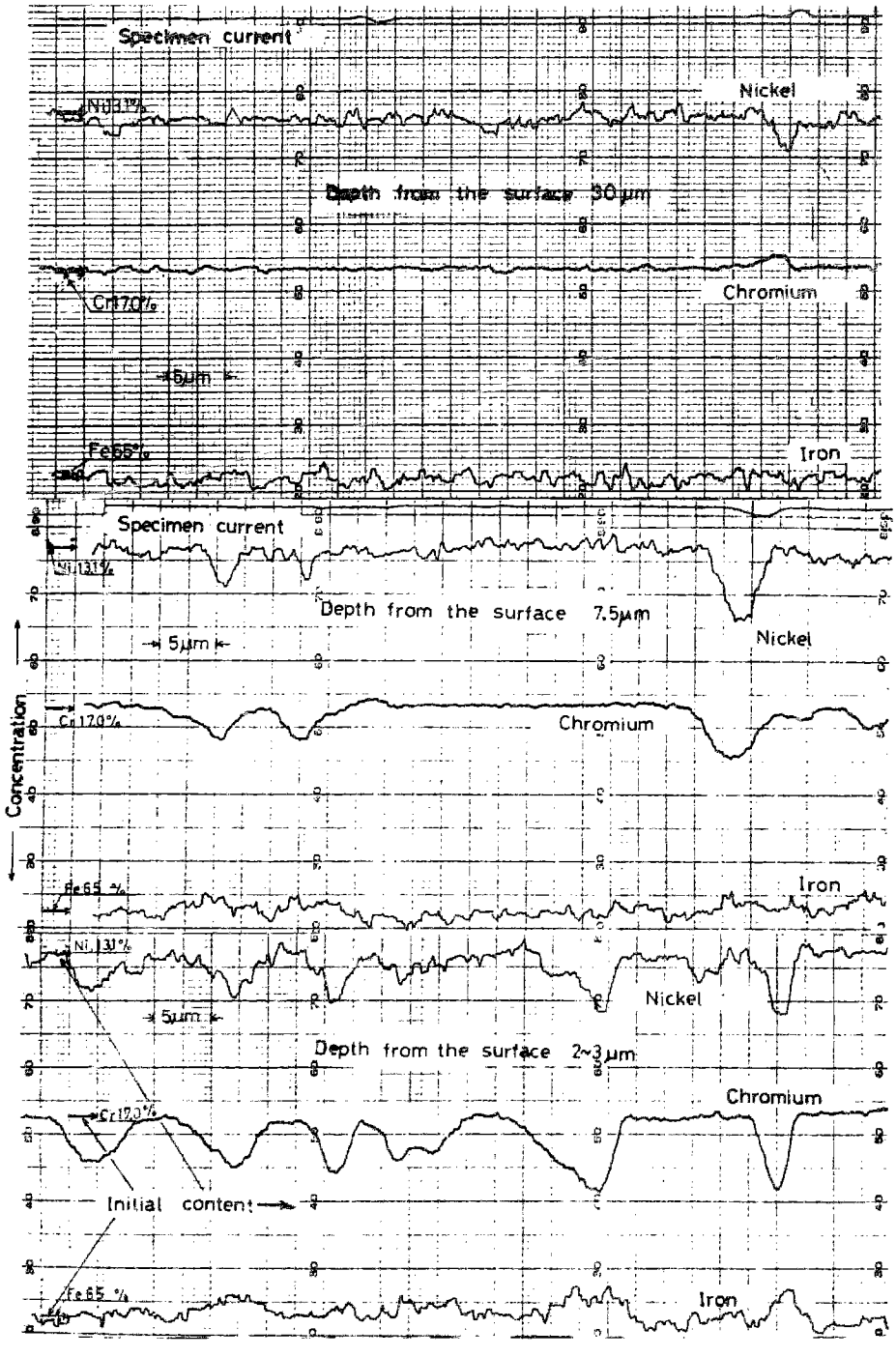

Fig. 13 Element depletion in the neighbour of sodium exposed surface of Type-316 stainless steel cladding tube specimen after 1000 hours in flowing sodium at 650°C (12 ppm O_2).

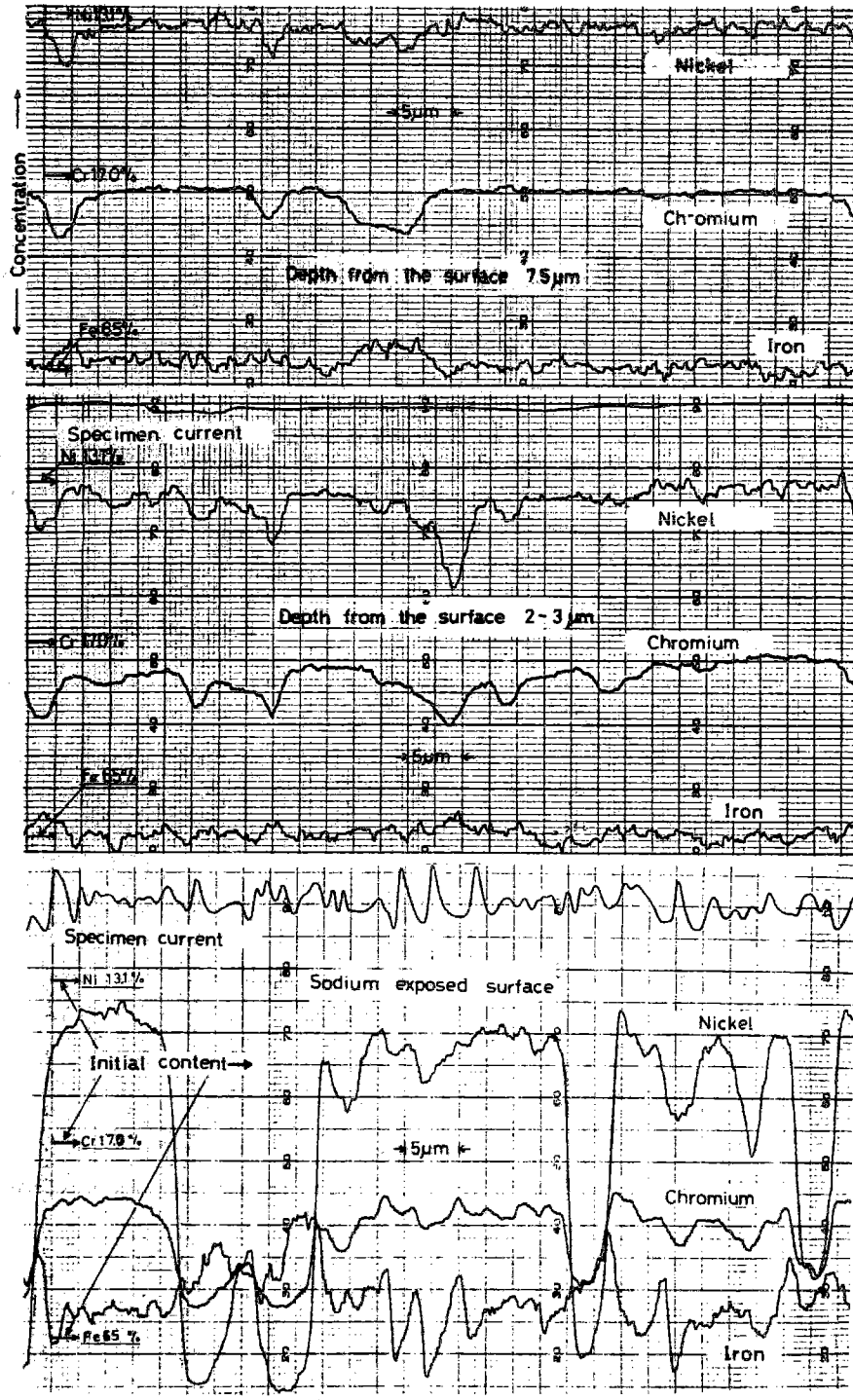

Fig. 14 Element depletion in the neighbour of sodium exposed surface of Type-316 stainless steel cladding tube specimen after 2000 hours in flowing sodium at 650°C (5 ppm O_2).

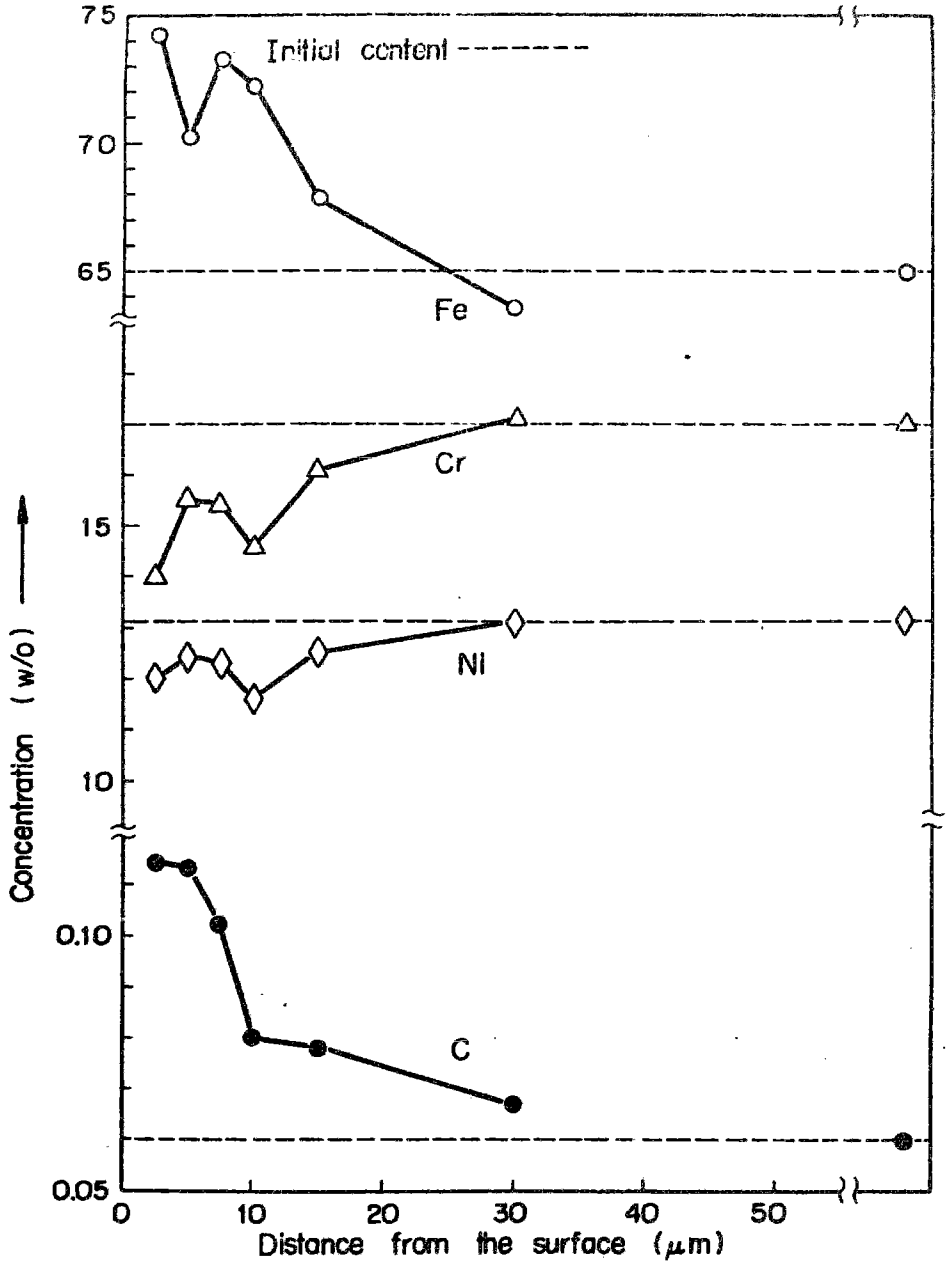

Fig.15. Element depletion in the neighbour of grain boundary (Fe, Ni, Cr) and in the matrix (C). Type-316 stainless steel cladding tube specimen after 1000 hours in flowing sodium at 650°C (12 ppm O_2) .

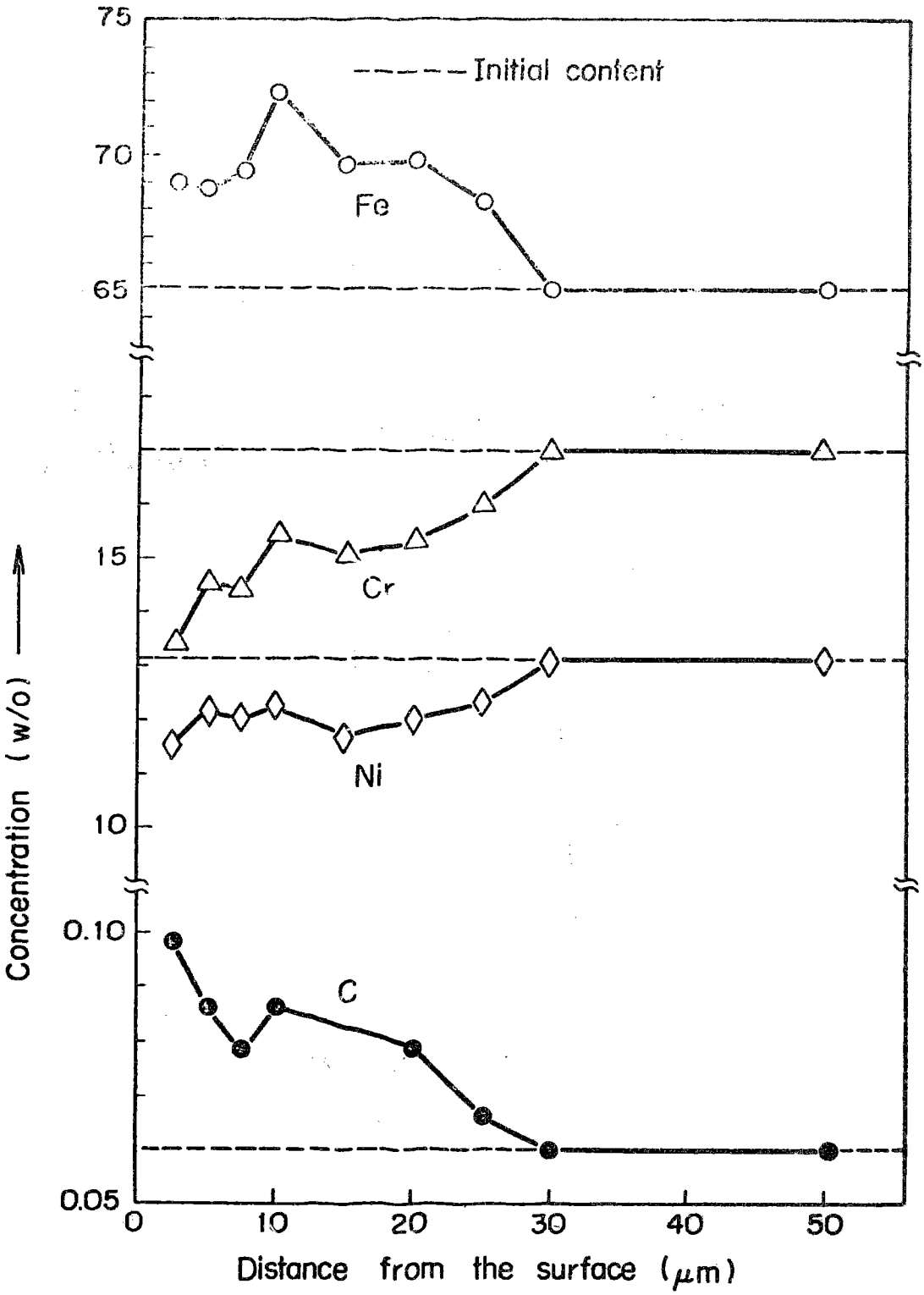

Fig.16. Element depletion in the neighbour of grain boundary (Fe, Ni, Cr) and in the matrix (C). Type 316 cladding tube specimen after 2000 hours in flowing sodium at 650°C (5 ppm O_2) .

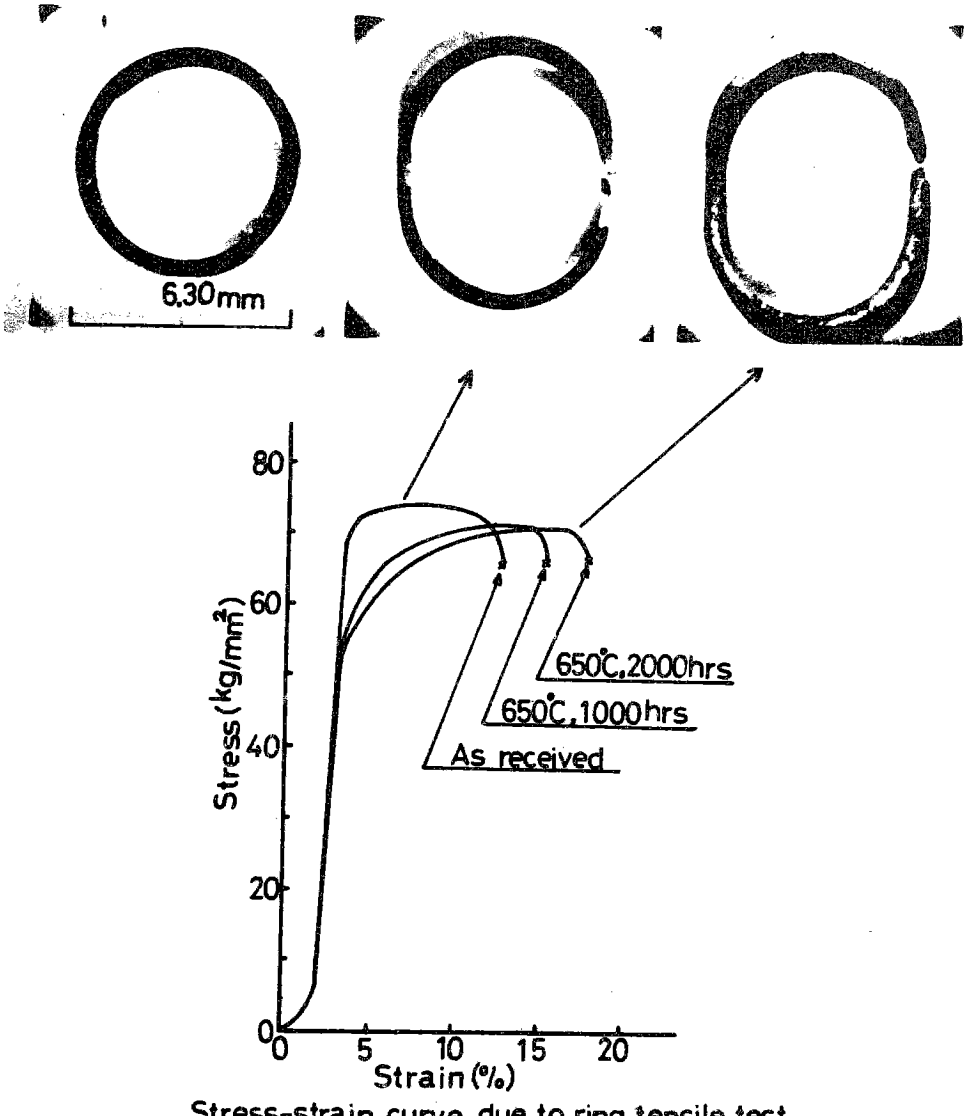

Fig. 17 Appearance of specimens after ring tensile test and stress-strain curve.

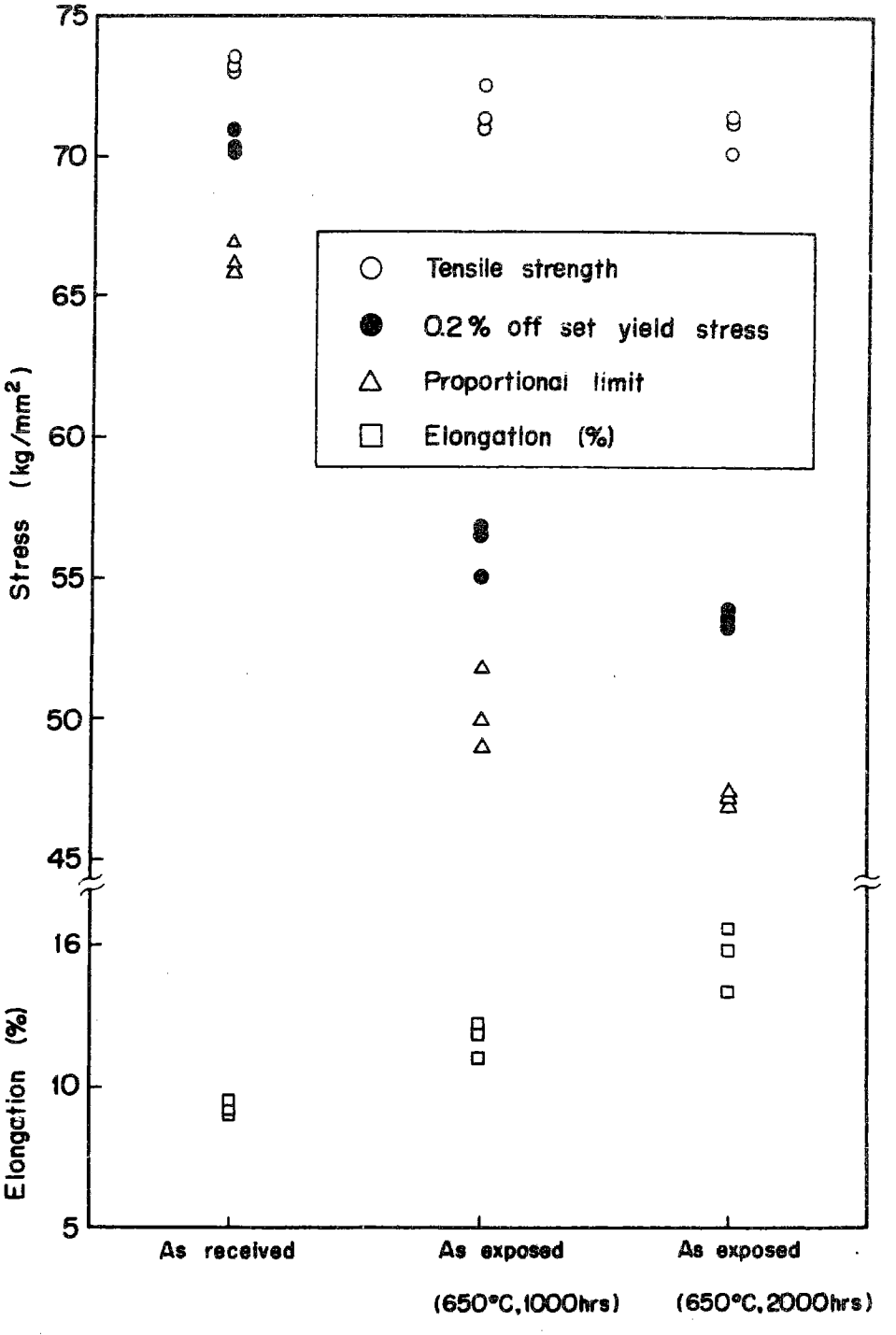

Fig.18. Change of mechanical properties due to ring tensile test of the stainless steel cladding tube specimen after exposure in 650°C sodium.

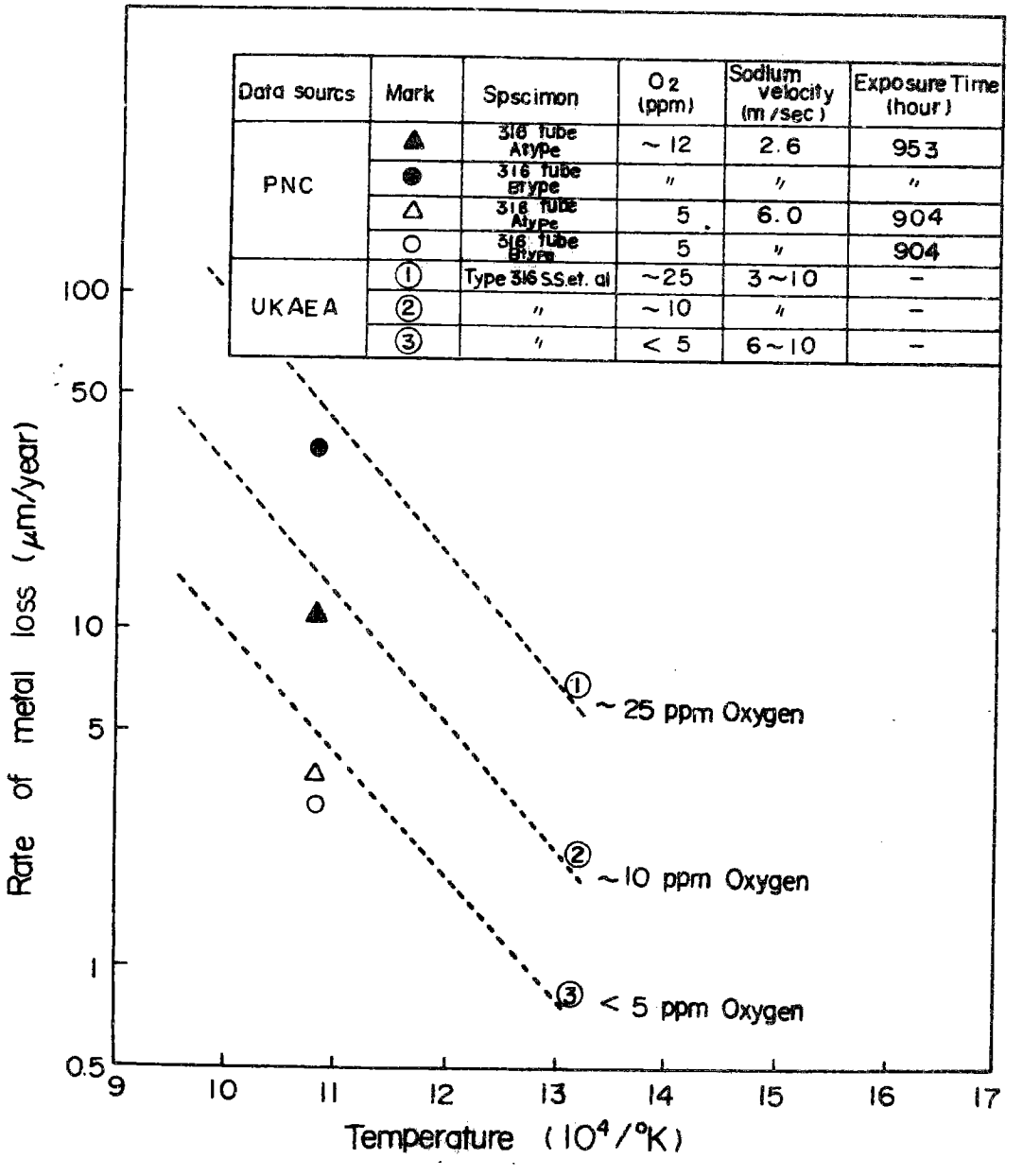

Fig.19. Metal-loss rate of Type-316 cladding tube specimen in 650°C sodium.

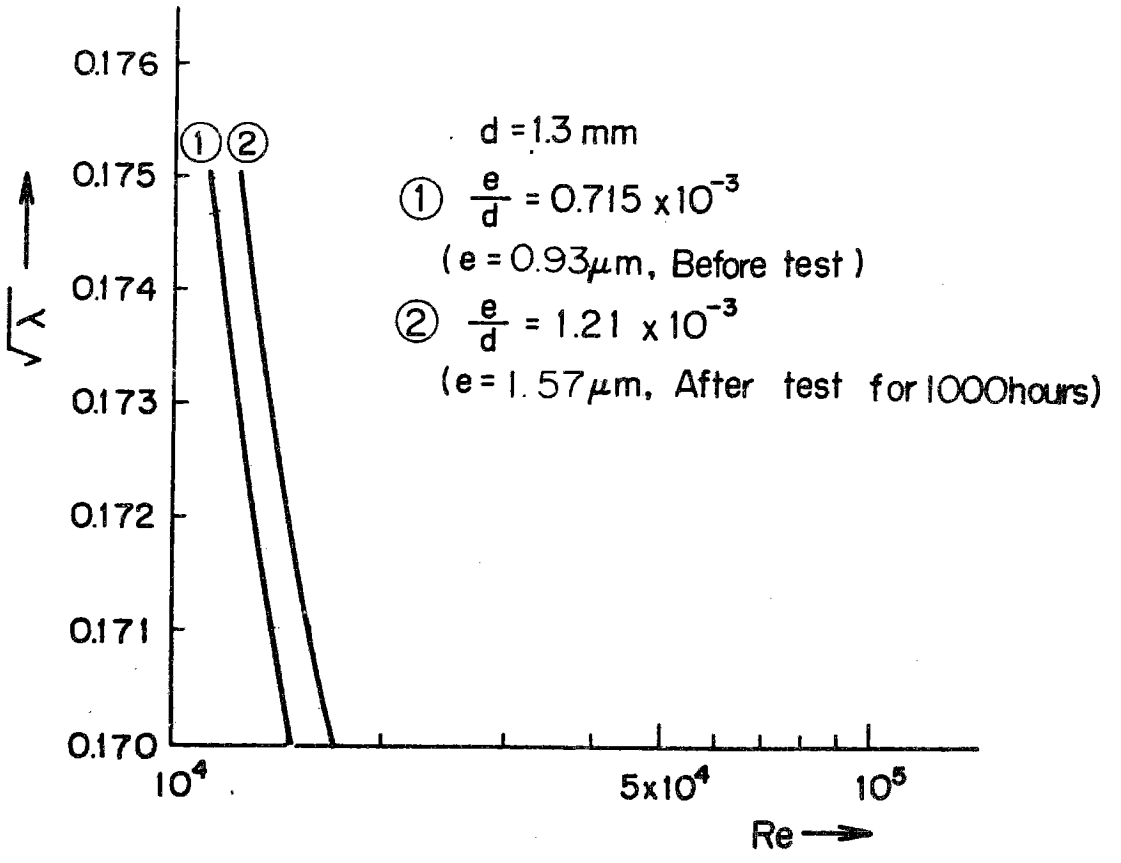

Fig.20. Relation between Re and $\sqrt{\lambda}$ (in M-2 loop).

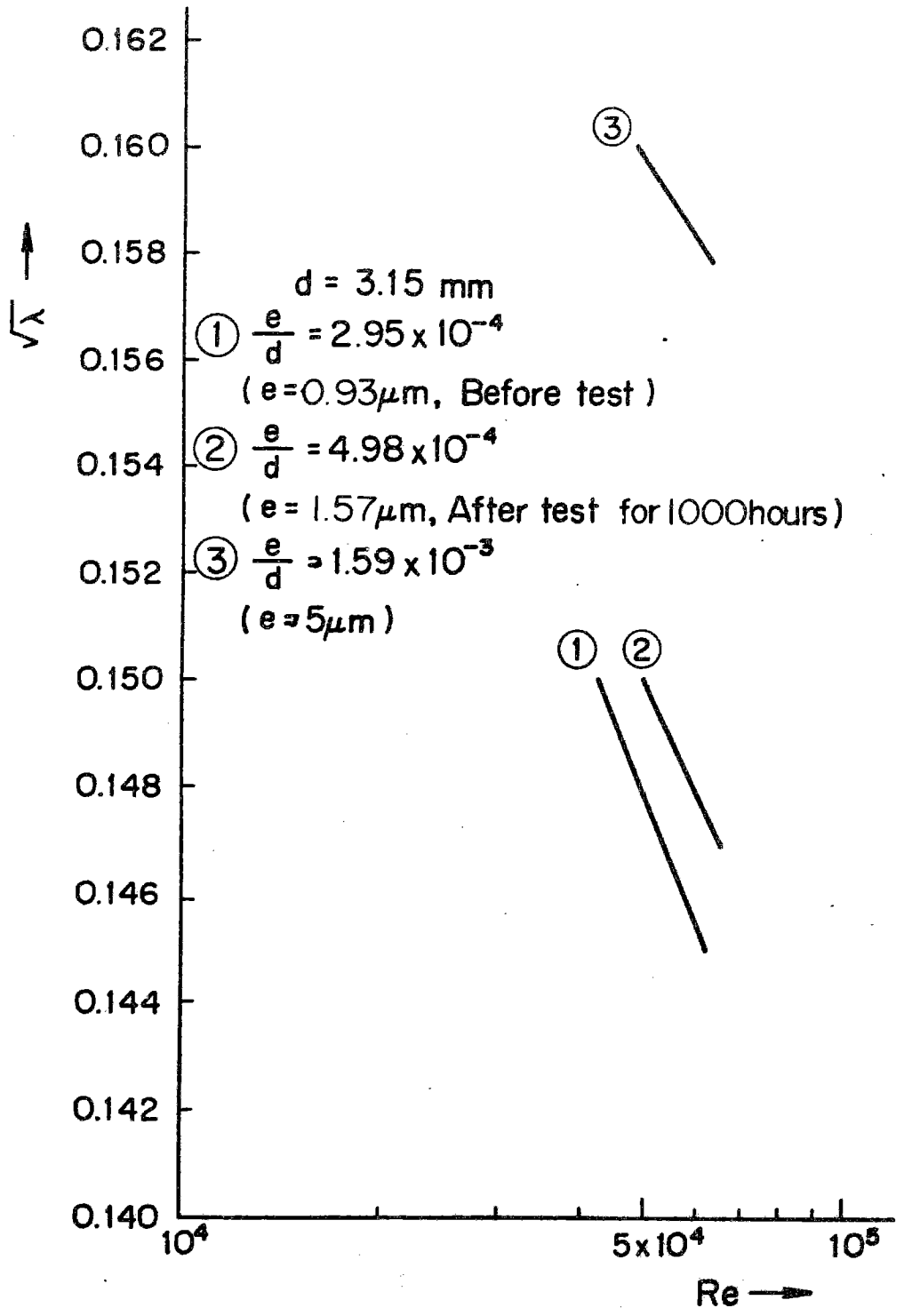

Fig.21. Relation between Re and $\sqrt{\lambda}$ (in JOYO).

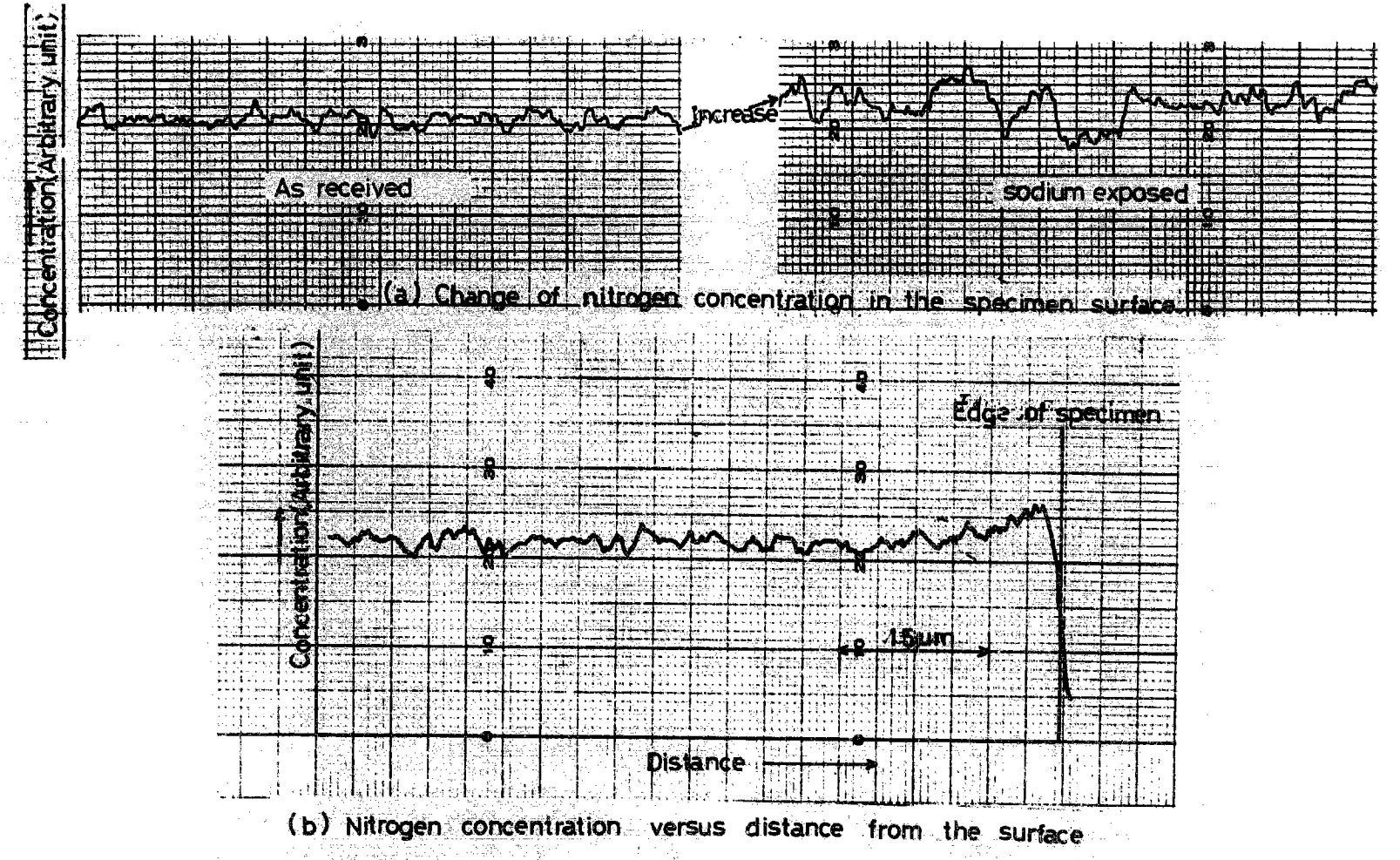

Fig. 22 Xray microprobe analysis of nitrogen of Type-316 cladding tube specimen after 2000 hours in flowing sodium at 650°C (5 ppm O_2).

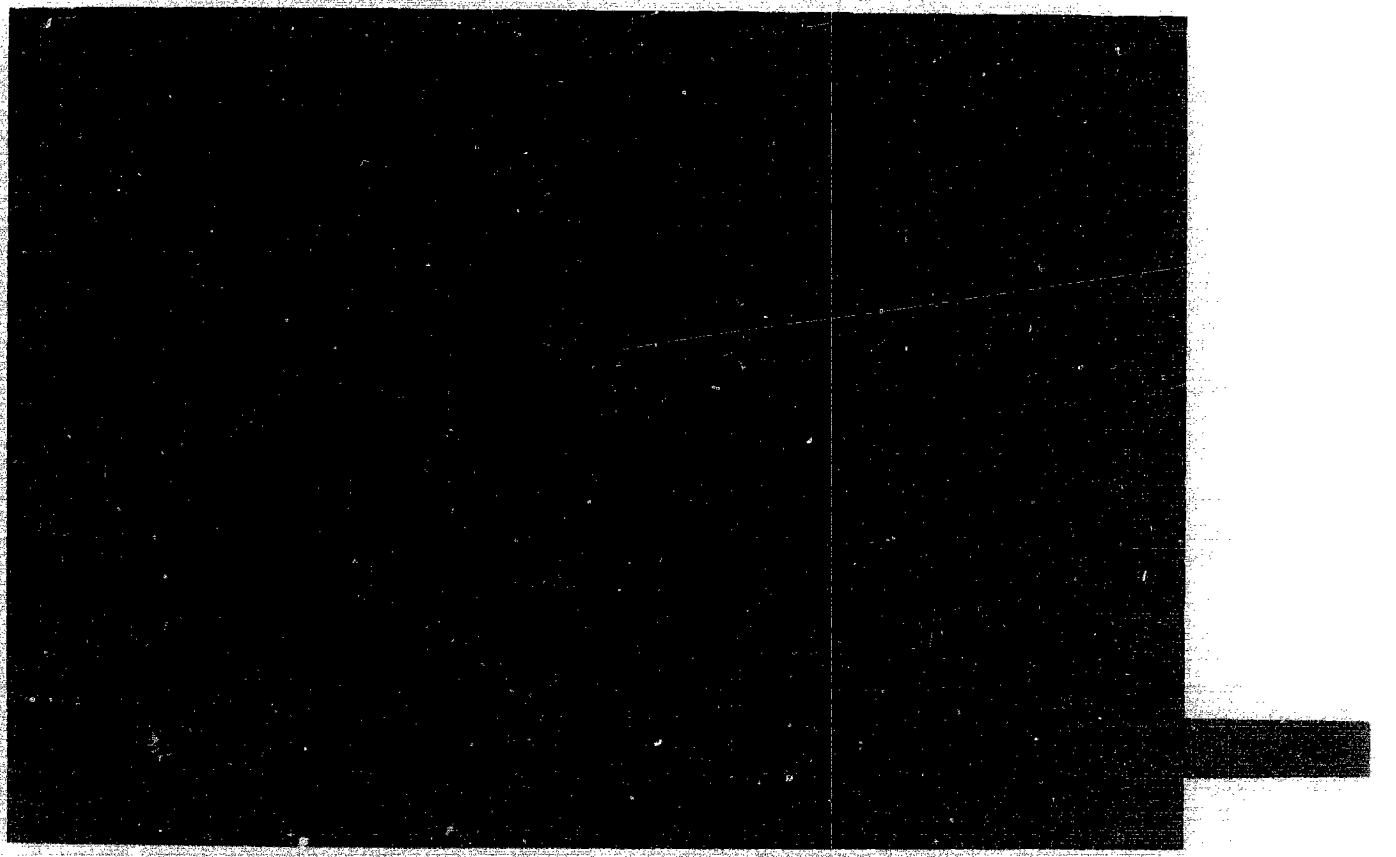

Photo-1. Appearance of M-11.

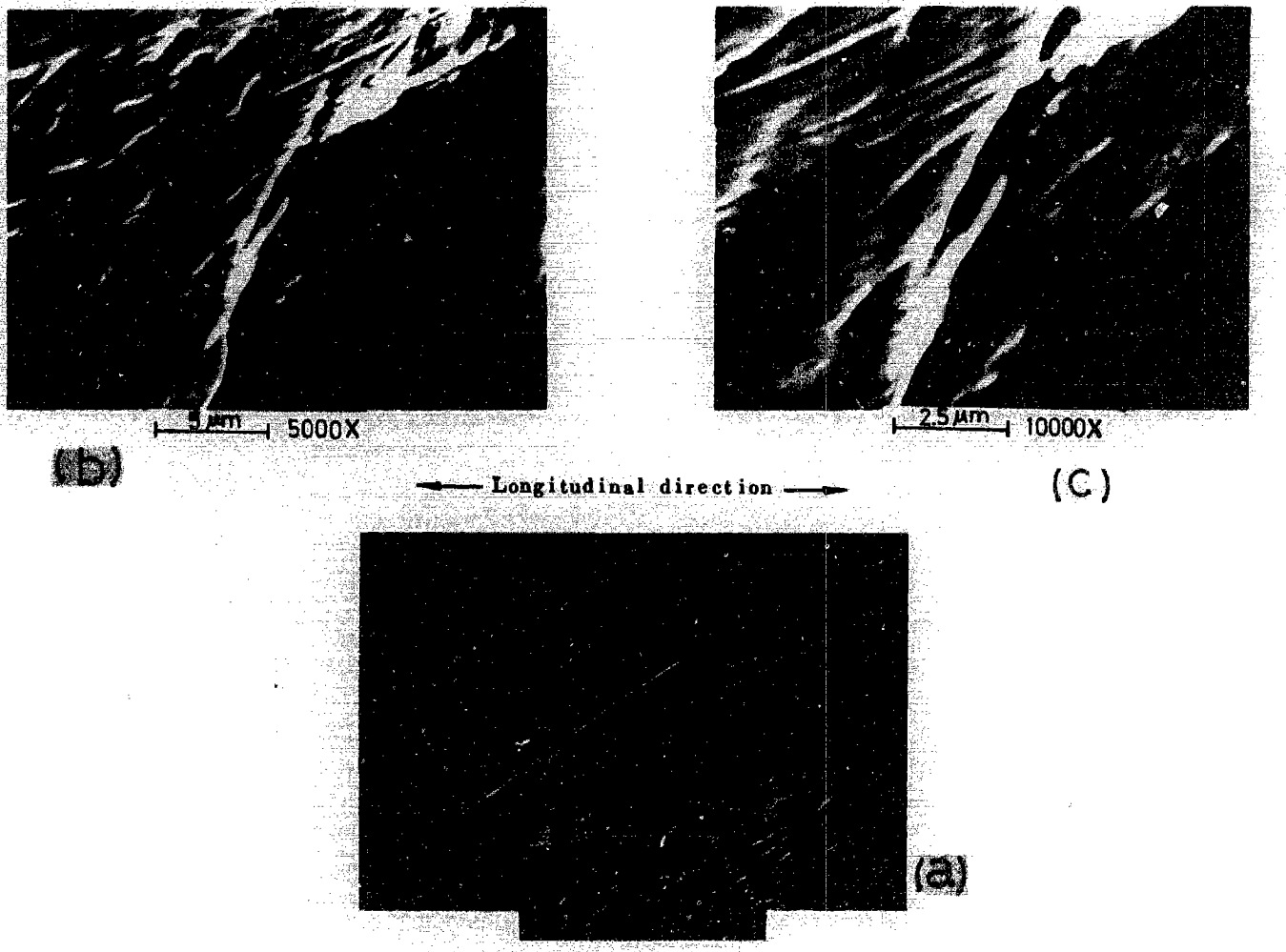

Photo-2. Scanning electron micrographs of Type 316 stainless steel cladding tube specimen before sodium exposure.

Surface after exposure for 1000 hours ($12ppmO_2$)

Surface of welding heat-affected zone after exposure for 1000 hours ($12ppm\ O_2$)

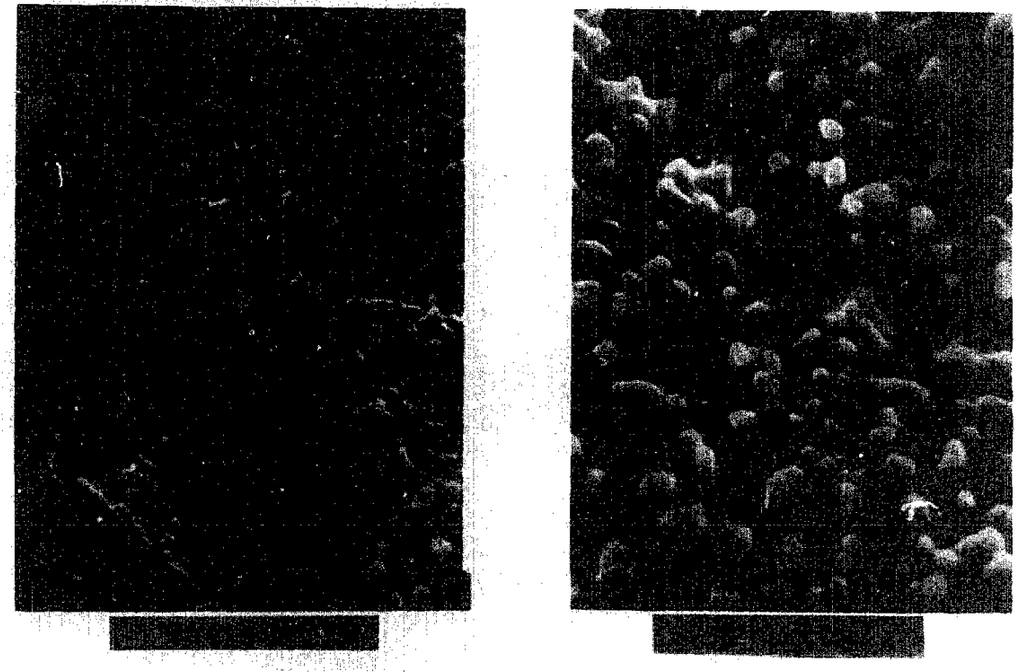

Surface after exposure for 2000 hours. (5ppm)

Photo-3. Scanning electron micrographs of Type 316 stainless steel cladding tube specimen surface after exposure in flowing sodium at 650°C.

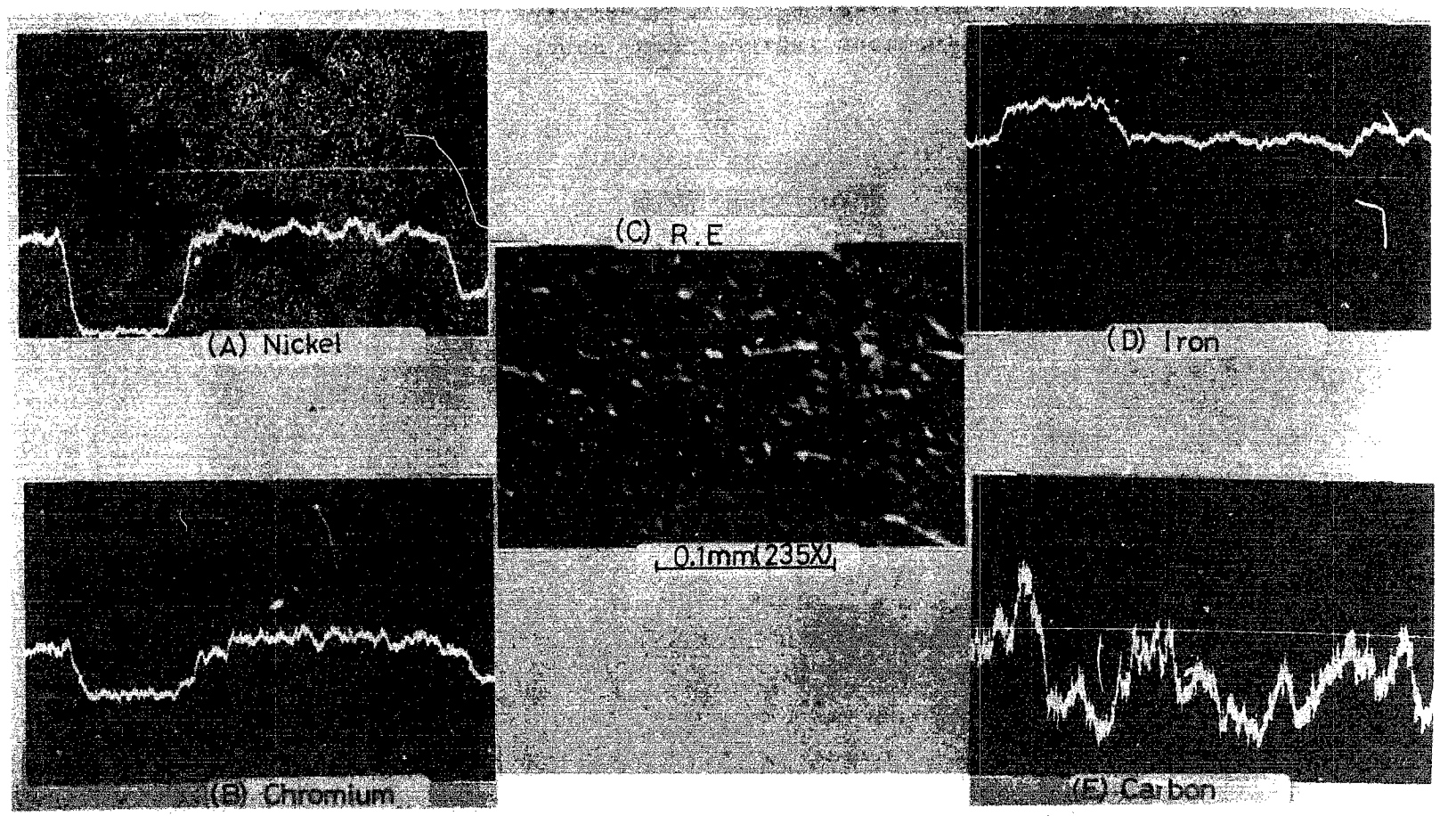

Photo-4. Xray micrographs of the specimen surface after exposure in following sodium at 650°C for 2000 hours.

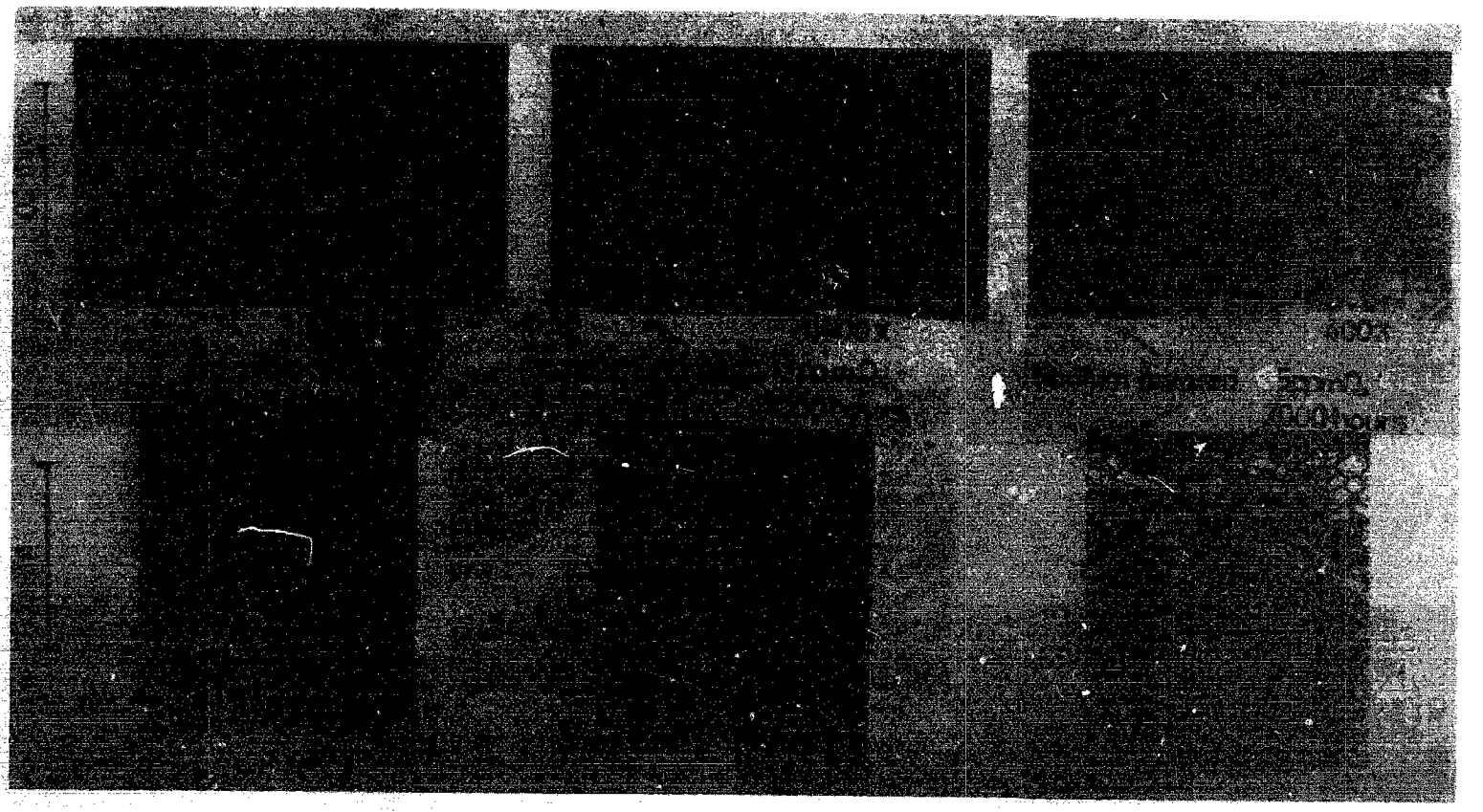

Photo-5. Photo-microstructures (Longitudinal section) of Type-316 stainless steel cladding tube specimen before and after sodium exposure.

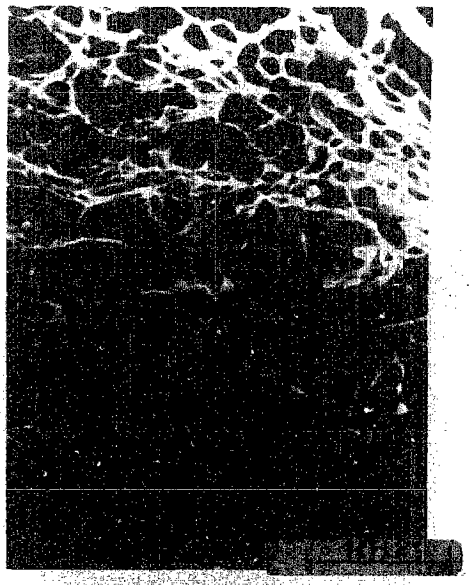

(A) Fractograph of the specimen as received. 3000×

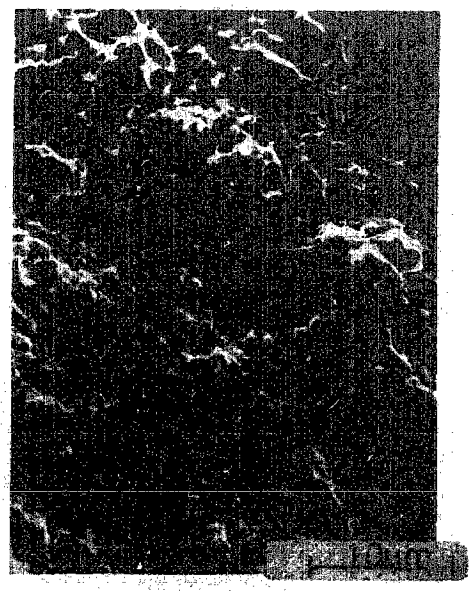

(B) Fractograph of the specimen as exposed in sodium. 3000×
(1000hr, 12ppmO_2)

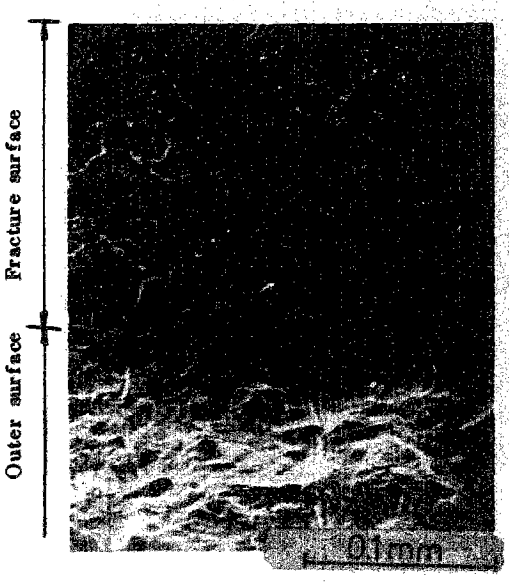

(C) Appearace of fracture surface of the specimen as received.
400×

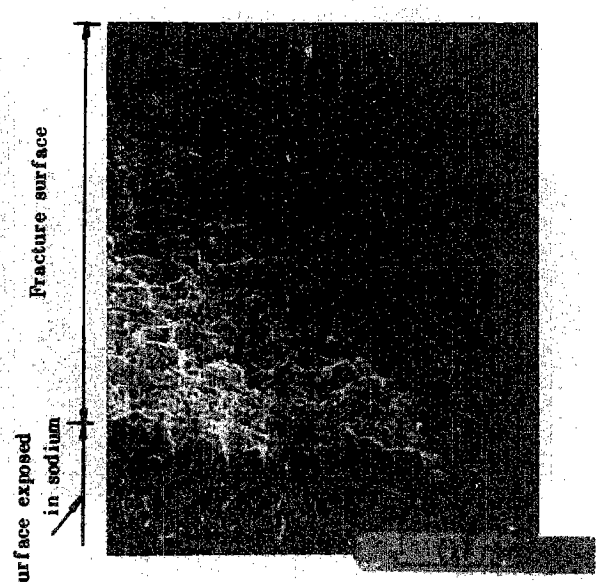

(D) Appeavance of fracture surface of the specimen aseexposed in sodium.
400× (1000hr, 12ppmO_2)

Photo-6. Fractographs of Type-316 stainless steel cladding tube specimen after ring tensile test at room temperature.

Photo-7. Photomicrographs of tensile-rupture specimens (Type-316 stainless steel).

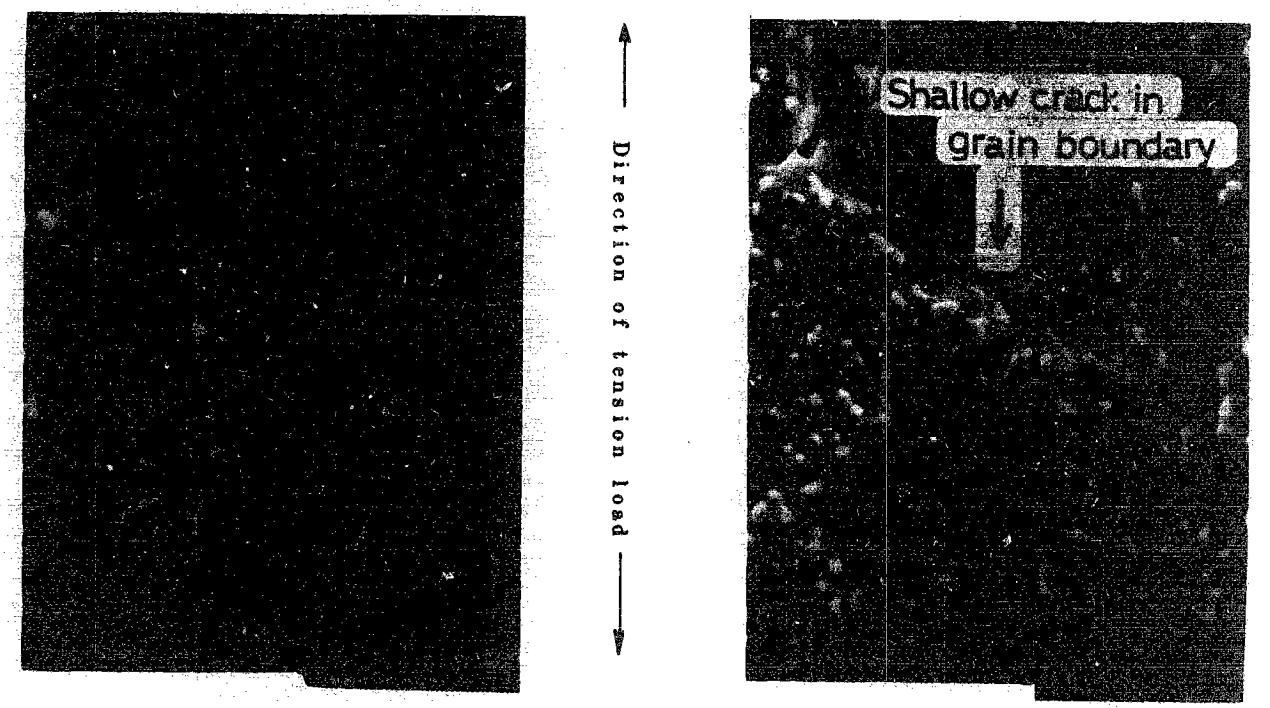

(A) 100hr, 12ppm O_2, 5000×

(B) 2000hr, 5ppm O_2, 5000×

Photo-8. Scanning electron micrographs of the outer surface in the neighbour of fracture after ring tensile test of the specimen exposed in sodium.